PRAYAS

Students' Journal of Physics

Volume 3 Number 6 Nov.-Dec., 2008

INDIAN ASSOCIATION OF PHYSICS TEACHERS

PRAYAS

Students' Journal of Physics

This is a bimonthly journal published by Indian Association of Physics Teachers. It publishes research articles contributed by Under Graduate and Post Graduate students of colleges, universities and similar teaching institutions, as principal authors.

Indian Association of Physics Teachers [IAPT]

Central Office :

Indian Institute of Education campus
128/2 J.P. Naik Road, Kothrud, Pune - 411 038
E-mail : centraloffice@iapt.org
prayas_iapt@yahoo.co.in
Phone : 91 20 2545 5504

Registered Office :

L 117/302, Naveen Nagar, Kanpur - 208 025

Manuscripts may be submitted in appropriate format to any of the editors. Manuscripts can also be sent directly to prayas@iopb.res.in.

For more information about subscription, membership, renewals, address changes, etc., enquiries should be addressed to the Managing Editor.

Editorial

Science and Cultural Force

After sixty years of independence of the country, it is a legitimate question to ask what contributions India has made to international science in general, and physics in particular, during these six decades; and how does it compare to the same in pre-independence era. While complacency tends to stagnate the growth process, the self introspection has the opposite effect of opening newer avenues for progress. Needless to say that in the pre-independence era, Saha, Bose, Bhabha, Raman and J. C. Bose made world class contribution comparable to the topmost peers in the respective fields and put India in the international map of science. Considering the upsurge of national sprit with the dawn of freedom, and massive investment in the expansion of education, it is but natural to expect a loftier attainment in science. Although the country has made a big stride in science and technology in many fields, this expectation has not been adequately belied.

The foundation of western system of education was laid with the establishment of the three universities at Calcutta, Bombay and Madras in 1857, with emphasis to produce clerks and officials to help in the colonial administration. Formal teaching of science commenced towards the end of the nineteenth century. Yet, within a span of half a century or so, the system produced such luminaries of scientists that too indigenously with scant or nominal resources should be considered mind boggling. What is the mystery behind this phenomenon? The historian may explain it as an effect of renaissance, but more concretely it is due to operation of an invisible force which may be termed as a cultural force. The late nineteenth century and the first half of twentieth century saw the emergence of a new ethos in the country in the form of struggle for freedom infusing the mass with the sprit of dedication, sacrifice, patriotism and above all an urge for excellence. Those who did not directly participate in the independence movement and worked in the areas like science, literature, art etc. had to console themselves by excelling in their chosen fields.

Besides the above cultural force which can be considered as internal, being characteristic of contemporary Indian society, there was an external force at work in the country. It is the British science culture. India was a colony of Britain since 1757 and as such formed a part of the British Empire, and therefore shared its culture in science. The microscopic number of teachers in colleges and universities in India, who were practicing science, were regarded as member of the science fraternity of Britain. Up to the end of Second World War, Britain was the centre of gravity of international science and Proceedings of Royal Soci-

ety was regarded as the core international journal. It was fairly easy for Indian scholars to get access to leading British universities. The Indian scientists were also getting patronage from their British counterparts in adequate measure.

The Nobel Prize of C. V. Raman would have slipped to Russian physicist but for the timely support of Ernest Rutherford from Cambridge. The story of legendary mathematician Ramanujan is too well known to be repeated here. These two cultural forces acted in unison enabling the enterprising Indian scientists to overcome the formidable barriers of meager opportunity and isolationism in their home country and achieve laurels of high order in international science.

Today India has about 500 universities, compared to meager 17 universities at the time of independence. It has about 20,000 colleges, more than a dozen of IITs and IISERs and a couple of hundred specialized institutions dedicated to research and strong national commitment for liberal support. There is a clamour in various fora that good students are not opting for career in research but preferring more lucrative professions in IT, Medical and Engineering etc. In research and innovation Indias performance is disappointing. In a survey of 130 countries, it is ranked only 41 in the innovation index with Malaysia and China ranking at 25 and 37 respectively and Singapore and Korea in the top 10. Massive investment in higher education and research is offered as the panacea for this dismal situation. Although it is only a part of the remedy the core of the problem is the weak cultural force pervading our academic institutions. An atmosphere bereft of fear, oppressiveness, hatred, jealousy and feudalism but charged with dedication urge for creativity, high academic values, mutual love and respect; fraternity feeling and cooperativeness can be created only by the teachers and scientists working in the institutions which no outside agency or abundance of funding can achieve. This is the soul of the institutions while the body is the physical infrastructure generated by money only. Such a cultural force nurtured and nourished over years can become traditions inspiring its members and lifting them upwards in the realm of higher academic attainment. Any short time visitor to such institutes will feel uplifted and inspired coming under the spell of such atmosphere. Harvard and Cambridge have been successful in creating it over centuries of dedication by its members. Institutes of modest means and infrastructure have achieved excellence and acquired laurels in the past and are continuing to do so in the present time on the strength of such cultural force.

L. Satpathy

P R A Y A S
Students' Journal
of Physics

TURNING POINTS

Solar Seismology & Solar Neutrinos

S.M. Chitre
DAE-Centre for Excellence in Basic Sciences, University of Mumbai, Mumbai

Abstract. The Sun has been aptly described as the 'Rosetta Stone' of Astronomy, and its internal and external layers have provided an ideal cosmic laboratory for testing atomic and nuclear physics, high-temperature, plasma physics and magnetohydrodynamics, neutrino physics and even general relativity. Even though the interior of the Sun is not accessible to direct observations, it is nonetheless possible to unravel its internal constitution with the help of equations of mechanical and thermal equilibrium governing its structure together with the boundary conditions provided by observations. The outstanding question is the correctness of the theoretically constructed solar models. As it turns out the solar interior is transparent to neutrinos released in the thermonuclear reaction network operating in the energy-generating core and also to seismic waves generated throughout the solar body, and these serve as complementary probes furnishing reasonably accurate information about the inside of the sun.

1 INTRODUCTION

The sun has played a major role in the development of mathematics and physics over the past several centuries. Thus, Kepler's laws provided the framework for the planetary motions under the influence of the Sun's gravitational field, laying the foundation for the Newtonian mechanics. During the following centuries, Newton's theory of gravitation successfully explained the phenomena of planetary motions and the precession of their elliptical orbits. Indeed, by the end of nineteenth century the measurements were so refined that the unaccounted precession of Mercury's orbit was found to be close to 43 seconds of arc per century. The agreement between the prediction of the general theory of relativity and the observed precession of the perihelion of Mercury was considered a great triumph for Einstein's geometrical formulation of gravitation. Another remarkable prediction of general theory of relativity was the gravitational deflection of light rays from the background star grazing the solar limb, measured to a reasonable accuracy to have a value close to 1.75 arc seconds (twice the Newtonian value) during the total solar eclipse of 1919. Likewise, a longer transit time for radio waves propagating close to the Sun through its deep potential well, was also amply verified. It is evident that the Sun has played a significant role in providing the verification of tests of general relativity and its widespread acceptance.

The proximity of our star enables us to make a close enough scrutiny of its surface and the overlying atmosphere, providing extensive data of high spatial resolution about its surface features which is clearly not feasible for other stars situated far away from us. A century or so ago all that was known about the Sun was from the study of its visible layers and indeed, the early astronomers had noticed that the solar disk was dotted with dark blotches on its otherwise immaculate surface. These sunspots were, in fact, known to the Chinese and Greek astronomers, but it was Galileo who made scientific observations of the march of these dark regions across the solar disk. The appearance of these spots first in mid-latitudes ($\sim 30^\circ$) and the migration towards the equator in the cyclical manner with a period of approximately 11 years before their disappearance have been systematically recorded, resulting in the well known "Butterfly" diagram due to Maunder. Solar astronomers have still not fully understood the processes that drive the solar activity cycle as well as the reversal of the Sun's global magnetic field.

The solar atmosphere has a rich display of spectacular fireworks and complex phenomena which can be witnessed in their dazzling splendour during the occurrence of a total solar eclipse. Thus, we observe for a few seconds the chromosphere as a firey red ring around the disk just before and after totality, followed by the appearance of the pearly white solar corona which changes its shape synchronously with the activity cycle, forming a jagged ring around the Sun at the peak of the activity cycle, and transforming into plumes and streamers at the phase of solar minimum.

2 STRUCTURE OF THE SUN

In Solar Physics the early investigations were largely devoted to an extensive collection of spectroscopic data in order to study the surface chemical composition, temperature and pressure. The spectroscopy of the solar surface revealed the presence of spectral lines of elements such as carbon, nitrogen, oxygen, silicon, sodium, magnesium, iron, etc. The helium was, in fact, first discovered in the spectrum of the Sun before it's existena was known in the laboratory. The spectroscopy of the chromospheric regions overlying the solar photosphere, during a total solar eclipse, established that hydrogen is the most abundant element in the Sun with helium being the next with one in ten atoms and heavier elements at the level of approximately one percent.

With this knowledge of the surface chemical composition, solar physicists turned their attention to working out the internal structure of the Sun. It was widely believed for several centuries that the interior of the stars shielded by the layers of material beneath the visible surface will never be accessible. It is, therefore, a triumph of the theory of stellar structure that it has been possible to construct a reasonable theoretical model for inferring the physical conditions inside the Sun with the help of mathematical equations governing the mechanical and thermal equilibrium together with boundary conditions provided by observations.

Mechanical equlibrium:

$$\frac{dP(r)}{dr} = -\frac{Gm(r)}{r^2}\rho(r)$$

$$\frac{dm(r)}{dr} = 4\pi r^2\rho(r)$$

Here, $P(r)$ is the pressure, $\rho(r)$ the density and $m(r)$, the mass interior to the radius, r, for a spherically symmetric Sun.

Thermal equilibrium:

$$\frac{dL(r)}{dr} = 4\pi r^2\rho(r)\epsilon,$$

where ρ is the energy generation rate per unit mass and $L(r) = 4\pi r^2(F_{rad} + F_{conv})$ is the solar luminosity maintained by the nuclear energy generated throughout the solar interior. Here F_{rad} and F_{conv} are respectively the radiative and convective fluxes of energy.

Energy transport:

The energy generated by the nuclear reaction networks is transported from the central regions to the surface where it is radiated into the space outside. In the inner two-thirds of the solar interior by radius the energy transported by radiative processes is given by

$$F_{rad} = -\frac{4acT}{3k\rho}\frac{dT}{dr}$$

Here a is the Stefan-Boltzmann constant, c the speed of light and k the opacity of solar material. In the zone extending approximately one third of the solar radius below the surface the radiative temperature gradient becomes unstable to convection. The convective flax modeled in the simplified framework of a local mixing-length formulation is expressed as

$$F_{conv} = -k_t\rho\frac{ds(r)}{dr},$$

where k_t is the turbulent diffusivity and $s(r)$, the entropy.

The outstanding question was how to check the correctness of these theoretically computed solar models and indeed, to enquire how the Sun shines with the energy generation by thermonuclear processes in its central regions.

The advent of the high-speed computers enabled the numerical integration of structure equations with the auxiliary input of physics supplemented by appropriate physical boundary conditions. For this purpose the Standard Solar Model (SSM) has been widely used assuming the Sun to be a spherically symmetric object with negligible effects of rotation, magnetic fields, mass loss and tidal forces on its global structure. A quasi-stationary state is supposed to be maintained with the mechanical

and thermal equilibrium throughout the solar interior. The energy generation takes place in the solar core by nuclear reactions which convert hydrogen into helium.

NUCLEAR REACTION NETWORKS

Proton-proton chain

	$p + p \rightarrow d + e^+ + \nu_e$	$(\leq 0.42$ MeV$)$
	$p + e^- + p \rightarrow d + \nu_e$	$(1.44$ MeV$)$
	$p + d \rightarrow {}^3He + \gamma$	
$pp - I$	${}^3He + {}^3He \rightarrow {}^4He + 2p$	
	${}^3He + p \rightarrow {}^4He + e^+ + \nu_e$	$(\leq\ 18.8$ MeV$)$
$pp - II$	${}^3He + {}^4He \rightarrow {}^7Be + \gamma$	
	${}^7Be + e^- \rightarrow {}^7Li + \nu_e$	$(0.38,\ 0.86$ MeV$)$
	${}^7Li + p \rightarrow {}^8Be + \gamma$	
	${}^8Be \rightarrow 2^4He$	
pp - III	${}^3He + 4He \rightarrow {}^7Be + \gamma$	
	${}^7Be + p \rightarrow {}^8B + \gamma$	
	${}^8Be \rightarrow {}^8Be + e^+ + \nu_e$	$(\leq 14.6$ Mev$)$
	${}^8Be \rightarrow 2^4He$	

Carbon-Nitrogen-Oxygen cycle

${}^{12}C + p \rightarrow {}^{13}N + \gamma$	
${}^{13}N \rightarrow {}^{13}C + e^+ + \nu_e$	$(\leq\ 1.2$ MeV$)$
${}^{13}N + p \rightarrow {}^{14}N + \gamma$	
${}^{14}N + p \rightarrow {}^{15}O + \gamma$	
${}^{15}O \rightarrow {}^{15}N + e^+ + \nu_e$	$(\leq\ 1.7$ MeV$)$
${}^{13}N + p \rightarrow {}^{12}C + {}^4He$	
or	
${}^{15}O + p \rightarrow {}^{16}O + \gamma$	
${}^{16}O + p \rightarrow {}^{17}F + \gamma$	
${}^{17}F \rightarrow {}^{17}O + e^+ + \nu_e$	$(\leq\ 1.7$ MeV$)$
${}^{17}O + p \rightarrow {}^{14}N + {}^4He$	$(\leq\ 1.7$ MeV$)$

The energy so generated in the central regions is transported outwards principally by radiative processes through bulk of the solar body, except for the region extending about a third of the solar radius below the photosphere where the energy flux in carried largely by turbulent convection modelled in the framework of a mixing length theory. It is assumed that there is no mixing of nuclear reaction products outside the convection zone, apart from the slow gravitational settling of helium

and heavier elements by the process of diffusion beneath the convection zone into the radiative interior. There is supposed to be no other mode of energy transport such as a wave motion and the standard nuclear and neutrino physics is adequate for designing solar models. The objective is to reproduce the present luminosity and radius after evolving the Sun, assuming the mass of the model is conserved with no accretion or mass loss.

In the theory of solar structure and evolution it is common to assume the mass of the Sun, $M_\odot = 1.989 \times 10^{33}$ gm and initial homogenous chemical composition, namely, hydrogen abundance by mass of 72%, helium by mass of 26% with a small admixture of heavy element abundance by mass 2%. The numerical computations, performed with two adjustable parameters, namely, the initial helium abundance and the ratio of the mixing length to the local pressure scale-height, then evolve the Sun to yield the present luminosity, $L_\odot = 3.846 \times 10^{33}$ erg s^{-1} and the radius, $R_\odot = 6.599 \times 10^{10}$ cm, after 4.6 billion years, the inferred age of the Sun. It turns out from the evolutionary calculations that there is a substantial variation of physical quantities across the solar body with the temperature varying from 5700 $^\circ$ K at the surface to upwards of 150 million degrees at the centre and likewise, the density changing by nine orders of magnitudes. The principal question confronting the theorists is whether there is any way of ascertaining these variations. Are there any means of measuring the central temperature and undertaking the chemical spectroscopy of the solar interior! This was very aptly described by Eddington: "At first sight it would seem that the deep interior of the Sun and stars is less accessible to scientific investigation than any other region of the universe. Our telescopes may probe farther and farther into the depths of space, but how can we ever obtain certain knowledge of that which is hidden behind substantial barriers? What appliance can pierce through the outer layers of a star and test the conditions within?"

3 WINDOWS ON THE SUN'S INTERIOR

31 Solar Neutrinos

The measurement of neutrinos present in the reaction network operating in the central regions of the Sun was the first probe conceived to infer the physical conditions in the solar core. The neutrino fluxes are very sensitive to the temperature and composition profiles prevailing inside the Sun. It was, therefore, expected that the steep temperature dependence of some of the nuclear reactions involved in the production of electron neutrinos would provide a handle to determine the Sun's central temperature to an accuracy of better than a few percent. The main thrust for setting up an experiment to measure the solar neutrino fluxes was "to see into the interior of a star and thus verify directly the hypothesis of nuclear energy generation in stars". Bruno Pontecarvo was the first scientist who made the proposal for using the chlorine detector for measuring the solar neutrino fluxes.

There have been valiant efforts undertaken since the 1960's to set up experiments designed for the exceedingly difficult measurement of neutrino counts from the Sun. Ray Davis's Chlorine experiment located some 4850 feet underground in the Homestake gold mine in South Dakota, USA

was the first such as attempt to count the solar neutrinos. It has a tank containing 615 tons of liquid perchloroethylene in which the chlorine nuclei serve as solar neutrino absorbers, sensitive to intermediate and high energy neutrinos, according to the reaction:

$$37_{C1} + \nu_e \rightarrow 37_{Ar} + e - (\text{threshold } = \ 0.814\,\text{MeV})$$

The Homestake solar neutrino experiment fulfilled the objective of the "use of a radically different observational probe to reveal wholly unexpected phenomena". In fact, Daxis's Chlorine experiment has been reporting measurements of the solar neutrino counting rate (2.56 $\pm$ 0.23 SNU, where 1 SNU = 10^{-36} captures per target atom per second) which are at variance with the count rate of 7.6 $\pm$ 1.2 SNU predicted by the Standard Solar Model. This puzzling deficit in the neutrino counting rate, by nearly a factor of 3 over the SSM prediction, constitutes the missing solar neutrino problem which had been haunting the community for well over three decades.

There have been a number of ingenious theoretical proposals to account for the observed deficit in the solar neutrino flux: partial mixing of material in the solar core which brings additional fuel of hydrogen and helium into the energy-generating regions, thus maintaining the nuclear energy production at a slightly lower temperature; the presence of a small admixture of Weakly Interacting Massive Particles (WIMP$_s$) in the solar core, effectively contributing to an increase in the thermal conductivity and in the process diminishing the temperature gradient required to transport the flux; a rapidly rotating solar core; a centrally concentrated magnetic field and even a lower heavy element abundance. All these proposals led to a slight reduction in the central temperature causing lowering of the high-energy neutrino flux.

A quarter of a century following the running of the Homestake Chlorine experiment, a Japanese set-up consisting of a 680 ton water tank was located about 1 km underground in the Kamioka mine was designed to detect charged particles by measuring Cerenkov light through the elastic scattering reaction (where x stands for electron, muon or tau neutrinos):

$$\nu_x + e^- \rightarrow \nu_x + e^-(\text{threshold } = \ 5\,\text{MeV})$$

The Kamioka and the upgraded Superkamiokande experiment are sensitive only to the high energy ^{8}B neutrinos released by the proton-proton chain of nuclear reactions. The measured flux from the Japanese experiment is again deficient by about a factor of 2 over the total flux predicted by the Standard Solar Model. It is evident that the Homestake and Superkamiokande experimental results are inconsistent with the proposition of resolving the solar neutrino puzzle with a lowering of the central temperature. Such a reduction in the central temperature will lead to even larger suppression of the high-energy ^{8}B neutrino flux to which the Superkamiokande experiment is exclusively sensitive because of the extremely high temperature dependence of the ^{8}B neutrino rate. The Homestake experiment detects the intermediate as well as high energy neutrinos from the Sun and paradoxically, records even a fewer neutrinos! Thus, we can eliminate a cooler solar core as viable solution for the solar neutrino problem.

Apart from these two set-ups there were three other radiochemical experiments: GALLEX, SAGE & GNO that use gallium detectors for the reaction:

$$^{71}Ga + \nu_e \rightarrow {}^{71}Ge + e^{-}(\text{threshold } = \ 0.233 \ rmMeV).$$

These are capable of detecting the low-energy pp-neutrinos, and report measurements of the solar neutrino counting rate, on an average of 74.7 ± 5.0 SNU. The predicted neutrino capture rate for the gallium experiments is 128 ± 8 SNU, again showing a deficit in the measured neutrino counting rate. Over the past four decades, carefully executed experimental efforts and increasingly more refined theoretical models have only confirmed the discrepancy between the measured and theoretically computed neutrino fluxes. It is now widely accepted that none of the three experimental results from Chlorine, Water Cerenkov and Gallium were consistent with one another, provided we assume the neutrinos to have standard physical properties, namely, no mass and hence no magnetic moment and no flavour-mixing during their journey from the site of generation in the energy-generating solar core to their detection here on Earth, and also that the Sun is in thermal equilibrium maintaining an unvarying luminosity. There are, in fact, general considerations independent of any underlying solar models which can demonstrably lead to unphysical situations such as a negative flux of beryllium neutrinos!

A possible resolution of this puzzling conundrum is to endow neutrinos with a tiny mass and permit the transformation of neutrino flavours during the course of their transit through the interior of the Sun and of the Earth, or through the interplanetary space in between. A direct consequence of such a proposal is that a fraction of electron neutrinos which are the exclusive by-products of the thermonuclear reaction network generating the solar energy would then go undetected in the existing solar neutrino experiments. This raises the exciting possibility of non-standard neutrino physics being responsible for the reported deficit in the measured neutrino fluxes and for invoking the need to go beyond the Standard Model of Particle Physics. The first compelling evidence for such neutrino oscillations and flavour mixing came from the analysis of Superkamiokande data on the high-energy cosmic ray - produced neutrinos in the terrestrial atmosphere. The Japanese experiment measured the difference in the up and down fluxes of neutrinos produced by the cosmic ray interaction with molecules in the Earth's atmosphere to demonstrate that neutrino oscillation, indeed, takes place during interaction with matter. This asymmetry in the up and down neutrino fluxes arises because of the passage of upward moving neutrinos through the solid mantle of Earth, while the downward moving neutrinos, coming from overhead after getting freshly generated in the terrestrial atmosphere, are less likely to undergo any flavour oscillations.

The measurements reported by the Sudbury Neutrino Observatory (SNO) seem to provide convincing evidence that the electron neutrinos generated in the solar core, indeed, change from one flavour to another during their journey from the Sun to Earth. The SNO experiment located at a depth of over 6000 meters in Sudbury, Canada uses 1000 tons of heavy water containing the deuterium isotopes of hydrogen for detecting solar neutrinos. Note the Superkamiokande detector uses ordinary water for capturing the neutrinos. In both the ordinary and heavy water, neutrinos can elastically scatter electrons to produce Cerenkov radiation, but such electron scattering can be caused by any of the three neutrino flavours: electron-, muon- and tau- neutrino. The Sudbury Neutrino Observatory is capable of measuring the 8_B neutrinos through the following reactions:

$$\nu_e + d \rightarrow p + p + e^{-} \qquad \text{(charged current)}$$

$$\nu_x + e^- \rightarrow \nu_x + e^- \qquad \text{(elastic scattering)}$$
$$\nu_e + d \rightarrow \nu_e + p + n \qquad \text{(neutral current)}$$

In both ordinary and heavy water detectors neutrinos can elastically scatter electrons to produce the Cerenkov radiation, but such electron scattering may be caused by any of the three neutrino flavours. However, SNO's heavy water detector is capable of isolating electron neutrinos, because that flavour alone can be absorbed by a deuterium nucleus to produce two protons and an electron. Note the neutral current reaction is equally sensitive to all the neutrino flavours, while the elastic scattering has significantly lower sensitivity to mu- and tau- neutrino flavours. Remarkably, SNO has reported the elastic scattering count rate which matches the Superkamiokande event rate to within experimental errors and SNO's count of the charged current reaction which is sensitive exclusively to the electron-neutrino flavour is lower than the SNO / Superkamiokande event rate recording all the three flavours. This unambiguous difference at the level of 1.666 in the 8_B flux deduced from the charged current and elastic scattering rates demonstrates that some of the electron neutrinos manufactured in the Sun's energy generating core are transformed into other types of neutrino flavours by the time they reach the experimental setups here on Earth. Furthermore, the total $8/_B$ neutrino flux as measured by the neutral current reaction in the SNO experiment is in satisfactory agreement with that predicted by the Standard Solar Model. These experimental measurements have reassured solar physicists that the simplified theoretical models of the Sun are essentially correct. Clearly, a resolution of the long standing solar neutrino problem should be sought in the realm of particle physics by endowing neutrinos with a tiny mass. It is worthwhile to recall that even though there is a remarkable agreement between the predicted neutrino production rates by the solar models and the direct measurement of neutrino counts by various experiments, we still have some processes ignored in the construction of the theoretical models, like the occurrence of possible mixing in the radiative interior, or the presence of a magnetic field concentrated in the solar core, or perhaps heat transport by waves or WIMP$_S$. Equally, some of the auxiliary input physics such as the nuclear reaction rates or the abundance of heavy elements and consequently, the opacity could be in error! This has prompted the community to explore an independent complementary tool to probe the physical conditions within the solar body and this was provided by the seismic studies of the Sun.

32 Solar Seismology

The solar surface undergoes a series of mechanical vibrations which are observed as Doppler Shifts oscillating with a period centered around 5 minutes. These have now been identified as acoustic modes of pulsation of the entire Sun. They represent a superposition of millions of standing waves with mode amplitude of the order of $\sim$ few cm/s with the frequencies of these modes determined to an accuracy of better than 1 part in 10^5. The accurately measured oscillation frequencies provide very tight constraints on the admissible solar models. This requires continuous observations over very long periods of time and is achieved with the help of ground-based networks like the Global Oscillation Network Group (GONG) comprising six stations located in contiguous longitudes around

the world, as well as with the satellite-borne instruments such as the Michelson Doppler Imager (MDI) on board the Solar and Heliospheric Observatory (SOHO).

A major task that was accomplished by inverting the accurately measured seismic data of oscillation frequencies was a fairly reliable inference of the acoustic structure of the Sun. The profile of the sound speed was determined through bulk of the solar interior to an accuracy of better than 0.1 % and the density profile to a somewhat lower accuracy. The agreement between the sound speed profile deduced from helioseismic inversions and the SSM is remarkably close except for a pronounced discrepancy near the base of the convection zone and a noticeable departure in the energy-generating core. The hump at the base of the convection zone may be attributed to a sharp change in the gradient of helium abundance profile on account of diffusion-which can smoothed out by a moderate amount of rotationally–induced mixing immediately beneath the convection zone. The dip in the relative sound speed difference between the inverted sound speed profile and that from SSM around r = 0.2 $R_\odot$ may be due to ill-determined composition profiles in the SSM, possibly resulting from the use of inaccurate nuclear reaction rates or our inadequate understanding of the diffusion process or even because of the presence of WIMP$_S$!

From the seismic data accumulated over the past decade the depth of the outer convection zone is deduced to be (0.2865 $\pm$ 0.0005) $R_\odot$ and the helium abundance in the solar envelope is estimated to be 0.249 $\pm$ 0.003. The seismic structure of the Sun so surmised was based on the equations of mechanical equilibrium, while the equations of thermal equilibrium have not be employed so far, largely because on oscillatory time scales of several minutes, the oscillatory, modes are not expected to exchange significant amount of energy. The solar oscillation frequencies are thus largely unaffected by thermal processes in the interior. Nevertheless, for determining the thermal and chemical composition profiles one needs to supplement the seismically inferred structure by the equations of thermal equilibrium together with the auxiliary input physics like the opacity of solar material, equation of state and nuclear energy generation rates. It is remarkable the inverted sound speed, density, temperature and composition profiles and consequently, the neutrino fluxes come out to be in close agreement with those given by the Standard Solar Model. A striking feature that emerges from these computations is that assuming standard properties of neutrinos but allowing for arbitrary variations in the input opacities and relaxing the requirement of thermal equilibrium, it turns out to be difficult to construct a seismic model that is simultaneously consistent with any two of the existing solar neutrino experiments within two standard deviations of the measured fluxes. This suggested that the persistent deficiency between measured and predicted solar neutrino fluxes was mostly likely due to the non-standard neutrino physics. It is, therefore, tempting to suggest that helioseismology may be regarded to have highlighted the importance of the Sun as a cosmic laboratory for studying the novel properties of neutrinos.

It should be noted that the inverted profiles also enable a determination of the luminosity of the Sun with the use of equation of thermal equilibrium. Such a computed luminosity may not, of course, match with the observed solar luminosity, $L_\odot$, and this discrepancy may be effectively utilized to provide a test of the input nuclear physics. In particular, it can be demonstrated that the cross-section of the proton–proton reaction needs to be increased slightly to (4.06 $\pm$ 0.07) $\times$ 10^{-25} MeV barn. The seismic model provides a handle on the central temperature of the Sun which is found to be (15.6

$\pm$ 0.4) $\times$ 10^6 $^\circ$K, allowing for upto 10% uncertainty in the input opacities (Antia & Chitre 1995). It can also help in determining the chemical composition profiles in the solar interior, The inferred helium profile turns out to be in reasonably good agreement with that in the SSM which incorporates diffusion into the radiative interior, except in the regions just beneath the convection zone where the profile is essentially flat. This is indicative of some sort of a mixing process operating possibly on account of a rotationally induced instability. It is interesting to recall that the temperature at the base of the solar convection zone is $\lesssim 2.2 \times 10^6$ $^\circ$K which is not high enough to burn helium. However, should there be some mixing of material extending a little into the interior to a radial distance of 0.68 $R_\odot$, temperature approaching 2.5×10^6 $^\circ$K will be reached for the lithium abundance observed at the solar surface.

Helioseismology has made it possible to determine the rotation rate in the interior from the accurately measured frequency splittings. The first order effect of rotation arising from the Coriolis force yields splittings which depend on odd powers of the azimuthal order, and these odd splitting coefficients can be effectively used to infer the rotation rate as a function of radius and latitude. Interestingly, it is found that the differential rotation observed at the solar surface persists through bulk of the convection zone; while in the radiative interior the rotation rate is largely uniform . There are two prominent shear layers: a sub-surface layer extending to a depth of about 35,000 km beneath the photosphere and a narrow transition region (tachocline) with a width of approximately 7000 km near the base of the convection zone.

The helioseismically inferred rotation rate is, indeed, consistent with the measured solar oblateness of approximately 10^{-5} . The resulting quadrupole moment then turns out to be (2.18 $\pm$ 0.06) $\times$ 10^{-7}, implying a procession of the perihelion of Mercury's orbit by about 0.03 arcsec / century, while the observed precession is close to 43 arcsec / century, thus clearly demonstrating tenability of the general theory of relativity. The even order terms in the splittings of solar oscillation frequencies represent the acoustic asphericity of the Sun. This presumably results from the presence of a large-scale magnetic field or a latitude-dependent thermal fluctuation in the solar interiors and this information should provide an effective probe of the eternal magnetic field of the Sun.

With accumulation of the helioseismic data from GONG and MDI for more than 11 years covering the cycle 23, it is now possible to study temporal variations in the solar interior with solar activity. It has, in fact, been demonstrated that the oscillation frequencies shift by upto 0.4 microhertz during the course of the cycle with the maximum frequency shift occurring near the peak of solar activity. Furthermore, the frequency variations are found to be correlated with various solar activity indices. It appears that most of the temporal variations in the solar structure are confined to a shallow subsurface layer and there is no significant change in the interior.

It is widely believed that the differential rotation plays a crucial role in driving of the solar dynamo and consequently, it is important to investigate temporal variations in the rotation rate. Indeed, time variation of the surface rotation rate with the solar cycle was earlier established by Howard & La Bonte . Their observations, in fact, demonstrated a surface pattern of torsional oscillations with bands of faster and slower than average rotation drifting slowly from mid-latitudes towards the equator and with a striking correlation with the magnetic "butterfly" diagram. It has now been possible with the available seismic data to study temporal variations of the rotation rate in the convection

zone. For this purpose the temporal average of the rotation rate at each radius and latitude is subtracted from the rotation rate, at any given epoch, inferred from inversion of the data over the relevant time interval to obtain the residual. This time-varying component of the rotation rate reveals a pattern similar to the torsional oscillations detected at the surface with alternating fast and slow bands migrating equatorward and poleward from the mid-latitudes and penetrating practically to base of the convection zone.

The current efforts in helioseismology are aimed at probing the magnetic field structure inside the Sun which should shed light on processes driving the cyclic magnetic activity and also locating the seat of the solar dynamo. It is hoped that the accumulating seismic data will enable us to study the temporal variation of acoustic mode frequencies and amplitudes reflecting the time-dependent changes in the solar structure and dynamics. In the process we may learn how the magnetic field configuration changes with the activity cycle and identify the mechanism responsible for causing the solar irradiance to vary synchronously with the sunspot cycle.

Yet, the present account will be incomplete without a reference to the recent downward revision of spectroscopic determination of solar photospheric abundances of Oxygen and other heavy elements causing a serious discrepancy between the standard solar models constructed with the new abundances and the seismically inferred model. This uncertain spectroscopic measurement of heavy element abundance, Z in the solar envelope has prompted efforts to determine seismically the value of Z which comes out to be 0.0172 ± 0.002 thus alleviating the discrepant results.

In conclusion, the two complementary probes, namely the painstaking measurement of solar neutrino fluxes and the accurately determined acoustic oscillation frequencies have demonstrated convincingly the remarkable concordance between the Standard Solar Model and the Seismic Solar Model. It then became evident that the long-standing solution for the solar neutrino problem is not to be sought in the realm of astrophysics, but rather in the domain of neutrino physics, implying neutrinos to have non-standard properties such as a non-zero mass.

References

[1] S. Eddington (1926): The Internal Constitution of the Stars (Cambridge University Press, Cambridge).

[2] S. Chandrasekhar (1930): An Introduction to the study of Stellar Structure (University of Chicago Press, Chicago).

[3] M. Schwarzschild (1959): Structure and Evolution of the Stars (Princeton University Press, Princeton).

[4] J.N. Bahcall (1989): Neutrino Astrophysics (Cambridge University Press, Cambridge).

[5] S.M. Chitre (2000): Perspectives on the Interior of the Sun, J. Astrophysics. Astr. 21, 331.

[6] H.M. Antia and S. Basu (2008): Reports on Progress in Physics.

P R A Y A S
Students' Journal
of Physics

Determining planetary positions in the sky for ± 50 years to an accuracy of 1° with a calculator

Tanmay Singal[1] **and Ashok K. Singal**[2]

[1] II Year B.Sc. Physics-Maths, St. Xavier's College, Ahmedabad, India. Email: tanmaysingal@gmail.com

[2] A & A Division, Physical Research laboratory, Ahmedabad, India. Email: asingal@prl.res.in

Abstract. In this paper, we describe a very simple method to calculate the positions of the planets in the sky. The technique used enables us to calculate planetary positions to an accuracy of 1° for ± 50 years from the starting epoch. Moreover, this involves very simple calculations and can be done using a calculator. All we need are the initial specifications of planetary orbits for some standard epoch and the time periods of their revolutions.

Communicated by A.M. Srivastava

1. INTRODUCTION

The night-sky fascinates people. To be able to locate a planet in the night sky is something that thrills people. Since the planets move with respect to the background stars and continuously change their positions in the sky, locating them in the sky could appear be a non-trivial task. It is a general notion that calculating the planetary positions is a very tedious task, involving a lot of complicated mathematical equations and computer work. However, to be able to locate planets in the sky one does not really need very accurate positions. After all, Kepler's laws, which describe planetary orbits reasonably well, are mathematically simple. Hence, one could use Kepler's law to predict planetary positions in which mutual influence of planets is not considered. Thereby an accuracy of $\sim 1^\circ$ in planetary positions would be achieved.

In this project, we employ a very simple method to calculate the positions of the planets. The technique we use enables us to calculate planetary positions to an accuracy of 1° for ± 50 years from the starting epoch. Moreover, this involves very simple calculations and can be done using a calculator. All we need are the initial specifications of planetary orbits for some standard epoch and their time periods of revolution. Although accurate planetary positions could be obtained easily from the internet, yet it is very instructive and much more satisfying to be able to calculate these ourselves, starting from basic principles and using a simple procedure.

Our first step would be to calculate the positions of all the planets (including Earth) in their orbits around the Sun. We initially consider the planets to revolve around the Sun in uniform circular

motions. Knowing their original positions for the starting epoch, we calculate their approximate positions for the intended epoch.

As a consequence of this approximation there will be an error since the actual orbits are elliptical. To get more accurate positions, we require some corrections, which are derived in Appendix A. These corrections account for the elliptical motion.

Knowing the positions of the planets around the Sun, we can then use simple co-ordinate geometry to transform their position with respect to an observer on Earth. Our task becomes simple since the orbits of all planets more or less lie in the same plane, viz. the ecliptic plane.

In this project, we calculate the motion of naked-eye planets only, although the procedure can be applied equally well for the remaining planets also.

2. CELESTIAL CO-ORDINATES

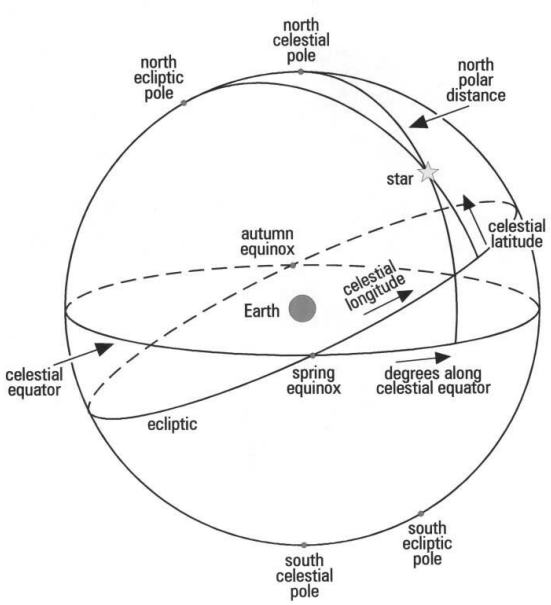

Figure 1. Celestial Sphere (see Reference 5)

All celestial bodies in the sky, including stars, planets, Sun, Moon and other objects, appear to lie on the surface of a giant sphere called the Celestial Sphere, see Fig. 1. Due to Earth's eastward rotation around its axis, the celestial sphere appears to rotate westward around Earth in 24 hours.

Infinitely extending the plane of Earth's equator into space it appears to intersect the celestial sphere to form a circle, which is called the Celestial Equator.

As Earth moves around the Sun, - as seen from the Earth - Sun changes its position with respect to the background stars. The path that Sun takes on the celestial sphere is called the "Ecliptic". The familiar Zodiac constellations are just divisions of the ecliptic into twelve parts. Since all the other planets revolve around Sun in nearly the same plane, they also appear to move on the ecliptic.

The celestial equator is inclined to the ecliptic by 23.5°. The points of intersections of these two circles on the celestial sphere are called the "Vernal Equinox" and the "Autumnal Equinox". The Vernal Equinox, also known as the Spring Equinox, is the point on the celestial sphere that the Sun passes through around the 21st of March every year.

In astronomy, an epoch is a moment in time for which celestial co-ordinates or orbital elements are specified, while a celestial co-ordinate system is a co-ordinate system for mapping positions in the sky. There are different celestial co-ordinate systems each using a co-ordinate grid projected on the celestial sphere. The co-ordinate systems differ only in their choice of the fundamental plane, which divides the sky into two equal hemispheres along a great circle . Each co-ordinate system is named for its choice of fundamental plane.

The ecliptic co-ordinate system is a celestial co-ordinate system that uses the ecliptic for its fundamental plane. The longitudinal angle is called the ecliptic longitude or celestial longitude (denoted λ), measured eastwards from 0° to 360° from the vernal equinox. The latitudinal angle is called the ecliptic latitude or celestial latitude (denoted β), measured positive towards the north. This coordinate system is particularly useful for charting solar system objects.

The Earth's axis of rotation precesses around the ecliptic axis with a time period of about 25800 years. Due to this, the equinoxes shift westwards on the ecliptic. Due to the westward shift of the Vernal Equinox, which is the origin of the ecliptic co-ordinate system, the ecliptic longitude of the celestial bodies increases by an amount $360/258 \sim 1.4^\circ$ per century.

Most planets, dwarf planets, and many small solar system bodies have orbits with small inclinations to the ecliptic plane, and therefore their ecliptic latitude β is always small. Due of the planets' small deviation from the plane of the ecliptic, the ecliptic longitude may alone suffice to locate planets in the sky.

3. CALCULATING PLANETARY POSITIONS

3.1 Heliocentric Circular Orbit

Here, we consider the planets to move around Sun in circular orbits with uniform angular speed. In Table 1, we have listed the period, T (days), of revolution of the planets (Nicholson, 1999). Then, the mean angular speed is give by, $\omega_0 = 360/T$ ($^\circ$/day).

To distinguish the Mean Longitude of the planet in the imaginary circular orbit from the *actual* longitude, λ we denote the former as λ_0.

Table 1. Mean longitude λ_0 on 01/01/2000, 00:00 UT and mean speed ω_0 of planets

Planet	Mean Longitude λ_0 ($^\circ$)	Revolution Period T (days)	Angular Speed ω_0 ($^\circ$/day)
Mercury	250.2	87.969	4.09235
Venus	181.2	224.701	1.60213
Earth	100.0	365.256	0.98561
Mars	355.2	686.980	0.52403
Jupiter	34.3	4332.59	0.08309
Saturn	50.1	10759.2	0.03346

The epoch values of mean longitudes (λ_0) of the planets given here (Table 1) are for 1st of January, 2000 A.D at 00:00 UT (adapted from Fränz and Harper, 2002).

We now demonstrate how to calculate λ_0 for Mars on 1st January 2007.

λ_0 of Mars on 01.01.2000 at 00:00 UT = 355.2° .

No. of days b/w 01.01.2000 and 01.01.2007 = 2557 days.

Mean angle traversed duration this period $= 0.52403 \times 2557 = 1339.9^\circ$.

So, λ_0 on 01.01.07 at 00:00 UT $= 355.2 + 1339.9 = 255.1^\circ$.[1]

In the same way, mean longitudes of all planets have been calculated in Table 2 for the same epoch. For a comparison, we have listed the actual longitude values (λ_e) from Indian Ephemeris (2007) for that epoch. Here, we see, from the difference in Column 4, that one has to correct for the elliptical shape of the orbit, at least for some of the planets.

Table 2. Mean longitude λ_0 on 01/01/2007, 00:00 UT

Planet	Mean Longitude λ_0 ($^\circ$)	Ephemeris value of Longitude λ_e ($^\circ$)	Difference ($^\circ$)
Mercury	274.3	268.7	+5.6
Venus	317.8	317.8	0.0
Earth	100.2	100.2	0.0
Mars	255.1	244.5	+10.6
Jupiter	246.8	242.6	+4.2
Saturn	135.7	140.2	-4.5

3.2 Heliocentric Elliptical Orbit

Before we make corrections for the elliptical shape of the orbit we need to know the orientation of the ellipse within the ecliptic and that can be defined by the longitude of the perihelion.[2] Lon-

[1] We have taken out the integer number of complete orbits.

[2] Perihelion is the point on the elliptical orbit closest to the Sun, while aphelion is the point farthest from Sun.

gitudinal distance of the planet in its orbit from the perihelion is known as its Anomaly (denoted by θ), while angular distance of mean position of planet with respect to the perihelion is called the Mean Anomaly (denoted by θ_0). As has been discussed in Appendix A, there is a one–to–one correspondence between θ and θ_0, and that the correction $\Delta\theta$ to be added to θ_0 (Equation 4) is,

$$\Delta\theta = 2\,e\sin\theta_0 + \frac{5}{4}\,e^2\sin 2\theta_0$$

where e is the eccentricity of the ellipse.

Let's consider Mercury on 01/01/07 at 00:00 UT.

Mean longitude, λ_0 = 274.3°

Perihelion Longitude, $\lambda_p = 77.5°$

Mean anomaly, $\theta_0 = \lambda_0 - \lambda_p = 196.8°$

1st order correction, $2e\sin\theta_0 = 2 \times 0.2056 \times \sin(196.8°) = -0.11885$ rad $= -6.8°$

2nd order correction, $\frac{5}{4}e^2\sin 2\theta_0 = 1.25 \times (0.2056)^2 \times \sin(33.6°) = 0.02924$ rad $= 1.7°$

$\Delta\theta$ = (1st order correction) + (2nd order correction) $= -6.8 + 1.7 = -5.1°$

Anomaly, $\theta = \theta_0 + \Delta\theta = 196.8 - 5.1 = 191.7°$

Precession of vernal equinox in 7 yrs $= 7 \times 360/25800 = 0.1°$.

$\lambda = \lambda_0 + \Delta\theta$ + precession of vernal equinox $= 274.3 - 5.1 + 0.10 = 269.3°$.

In the same way we can obtain the corrected longitudes for the remaining planets, which are listed in Table 3. Also listed are the longitude of perihelion, λ_p, mean anomaly, θ_0 and eccentricity e of elliptical orbits of planets (taken from Fränz and Harper, 2002).

Table 3. Corrected longitude λ on 01/01/2007, 00:00 UT

Planet	λ_0 (°)	λ_p (°)	θ_0 (°)	e	$\Delta\theta$ (°)	θ (°)	λ (°)	λ_e (°)	Error (°)
Mercury	274.3	77.5	196.8	0.2056	-5.1	191.7	269.3	268.7	0.6
Venus	317.8	131.6	186.2	0.0068	-0.1	186.2	317.9	317.8	0.0
Earth	100.2	102.9	357.3	0.0167	-0.1	357.2	100.2	100.2	0.0
Mars	255.1	336.1	279.0	0.0934	-10.8	268.3	244.5	244.5	0.0
Jupiter	246.8	14.3	232.4	0.0485	-4.2	228.2	242.6	242.6	0.0
Saturn	135.7	93.1	42.6	0.0555	4.5	47.1	140.3	140.2	0.1

From Table 3, we see that the errors now are indeed smaller than 1°.

3.3 Geocentric Perspective

Until now, we have calculated the longitudes λ of the planets on the celestial sphere centered on the Sun. We can also calculate radii r of their orbits around the sun, giving their positions in polar form (r, λ). To get the positions of planets on the celestial sphere centered on the Earth, we convert the polar co-ordinates into rectangular form and after shifting the origin from Sun to Earth, we change them back into polar form.

For converting into a rectanagular form, we have to decide upon the direction of the X and Y axes. We assume X to be in the positive direction along the line joining the Sun to the Vernal Equinox, and Y to be perpendicular to X in the ecliptic plane in such a way that the longitude is a positive angle.

3.4 An Example

As an example, this procedure is demonstrated for Mercury's position on 01/01/07 at 00:00 UT.

1 Heliocentric Co-ordinates

Distance, r, of Mercury from Sun can be obtained from anomaly θ as,

$$r = \frac{a(1-e^2)}{1+e\cos\theta} = 0.464\text{A.U.},$$

where $a = 0.387 A.U.$ is the length of semi–major axis of its elliptical orbit. Thus heliocentric polar co-ordinates of Mercury are (0.464 A.U., 269.3°). Then we can get heliocentric rectangular co-ordinates of Mercury as,

$X_h = r\cos(\lambda) = -0.006$ A.U.

$Y_h = r\sin(\lambda) = -0.464$ A.U.

Similarly we get heliocentric rectangular co-ordinates of Earth as,

$X_0 = -0.174$ A.U.

$Y_0 = 0.968$ A.U.

2 Geocentric Co-ordinates

Geocentric rectangular co-ordinates of Mercury then are

$X_g = X_h - X_0 = 0.168$ A.U.

$Y_g = Y_h - Y_0 = -1.432$ A.U.

Converting these into polar form, we get the geocentric distance and longitude as,

$r_g = \sqrt{(}X_g^2 + Y_g^2) = 1.442$

$\lambda_g = \tan^{-1}(Y_g/X_g) = 276.7°$.

We give the calculated geocentric longitudes, on 01.01.07 at 00:00 UT, of other planets in Table 4. Comparing with the geocentric longitudes from ephemeris λ_{ge}, it can be seen that the errors are much less than $1°$.

We have ignored any perturbations on the motion of a planet due to the effect of other planets which may distort its elliptical path. We are able to get the accuracy of $< 1°$ for long periods (± 50 years) because most of the terms ignored in the heliocentric longitude calculations are periodic in nature and do not grow indefinitely with time (see e.g., Simon et al, 1994). The other parameters

Table 4. Geocentric longitude λ_g on 01/01/2007, 00:00 UT

Planet	a (A.U.)	e	r (A.U.)	λ ($^\circ$)	r_g (A.U.)	λ_g ($^\circ$)	λ_{ge} ($^\circ$)	Error ($^\circ$)
Mercury	0.387	0.2056	0.464	269.3	1.44	276.7	276.5	0.2
Venus	0.723	0.0068	0.728	317.8	1.62	296.1	296.1	0.0
Earth	1.00	0.0167	0.983	100.2	–	–	–	–
Mars	1.52	0.0934	1.51	244.5	2.38	258.4	258.4	0.0
Jupiter	5.20	0.0485	5.36	242.6	6.17	248.2	248.2	0.0
Saturn	9.55	0.0555	9.17	140.3	8.44	144.6	144.5	0.1

characterizing the elliptical orbit, like the longitude of the perihelion, semi–major axis and eccentricity etc. change so slowly with time that for the accuracy we are interested in, these can be considered constant for ± 50 years.

4. LOCATING PLANETS IN THE SKY

Now that we have calculated the geocentric longitudes of the planets, we are in a position to locate them in the sky. Any one familiar with the Zodiac constellations could locate the planet from its position in the constellation in which it lies. The ecliptic is divided into 12 Zodiac signs – Aries, Taurus, Gemini, Cancer, Leo, Virgo, Libra, Scorpio, Sagittarius, Capricorn, Aquarius, Pisces. The Vernal equinox, a zero ecliptic longitude, is the start of the first Zodiac sign and is also known as the First Point of Aries. But there is a caveat here. Because of the precession the vernal equinox has shifted westward by almost the full width of a constellation in the last ~ 2000 years since when the Zodiac signs and constellation were perhaps first identified. As a consequence, the First Point of Aries now lies in the constellation Pisces. For example, on 01/01/2007, geocentric longitude 276.7° of Mercury implies it is in the 10th Zodiac sign, which lies in Sagittarius constellation, taking into account the shift by one constellation due to precession. There are further complications. The twelve constellations are not all of equal length of arc along the ecliptic longitude. Moreover there is another constellation, viz. Ophiuchus, through which the ecliptic passes. However these complications are somewhat set aside by the fact that there are only about half a dozen stars in the Zodiac with an apparent brilliance comparable to the naked–eye planets, therefore with some familiarity of the night-sky, one could locate the planets easily from their geocentric longitude values. It further helps to remember that unlike stars, the planets, because of their large angular sizes, do not twinkle.

For a more precise location of a planet we can calculate its relative angular distance from the Sun along the ecliptic. For this we would require the geocentric longitude of the Sun. The position of Sun on celestial sphere, as seen from Earth, is exactly in opposite direction to the position of Earth as seen from the Sun.

Geocentric longitude of Sun = Heliocentric longitude of Earth + 180°

The difference in the geocentric longitude of the planet from that of the Sun tells us about its apparent position in the sky with respect to the Sun. If the longitude of the planet is greater than the

longitude of the Sun then the planet's position lies to the east of the Sun. That means that its rise time will be later than that of the Sun and it will also set after the Sun. So the planet will be visible in the evening sky. On the other hand, if the geocentric longitude of the planet is smaller than of the Sun, it will rise before the Sun and set also before it. Hence, this planet will be visible in the morning sky towards the east. As a demonstration, position of Mars with respect to Sun on 01.01.07 at 00:00 UT is calculated here:

Geocentric longitude of Sun = 100.2 + 180 = 280.2° (from Table 4)

Geocentric longitude of Mars = 258.4° (from Table 4)

Since longitude of Mars is smaller than that of the Sun, it lies to the west of the Sun. Therefore Mars lies $\sim 22^\circ$ west of the Sun on the ecliptic on this date.

As Earth completes a rotation in 24 hours, the westward motion of the sky is at a rate 15°/ hour. This rate is strictly true for the celestial equator. However we can use this as an approximate rotation rate even for the ecliptic, which actually is inclined at a 23.5° to the equator. Therefore Mars will rise 22/15 $\sim$ about one and half hour before the Sun.

Similarly, Venus, which lies $\sim 16^\circ$ east of the Sun, will set on that day a little more than an hour after the sunset. This way, one can easily locate the planets in the sky by knowing their positions with respect to the Sun.

5. CONCLUSIONS

It is a general notion that calculation of position of planets in the night sky is a difficult job, which can be accomplished only by complex scientific computations, using fast computers. The motive of this project has been to bring out the fact that such complex and accurate computations are not always really necessary. One can calculate the position of planets using the method derived here and get the thrill of finding the planet at the predicted position in the night sky.

We have been able to obtain the position of planets within an accuracy of 1°, using a calculator. This method can be used to reckon planetary positions up to ± 50 years of the starting epoch.

ACKNOWLEDGEMENTS

Tanmay Singal expresses his gratitude to the Astronomy and Astrophysics Division, and in particular to Dr. Hari Om Vats, of the Physical Research laboratory Ahmedabad, where work on this project was done.

APPENDIX A: CORRECTING FOR THE ELLIPTICAL ORBIT

We compute the correction for motion of a planet in an actual elliptical orbit from that in an imaginary circular orbit.

Period of revolution in circular orbit is taken to be exactly the same as that in the elliptical orbit. The origin of the mean longitude in circular orbit is chosen such that λ_0 coincides with the longitude λ of the planet when it is at the perihelion in its elliptical orbit. For mathematical convenience, we take $t = 0$ at that instant. Then $\lambda_0(0) = \lambda(0)$. Let λ_p be the longitude of the perihelion of the planet's elliptical orbit. We subtract the λ_p from λ_0 and λ to obtain what is called the "mean anomaly" and "anomaly" respectively (denoted here by θ_0 and θ, respectively) of the planet. Then

Mean Anomaly, $\theta_0 = \lambda_0 - \lambda_p$,

Anomaly, $\theta = \lambda - \lambda_p$.

Then $\theta_0(0) = \theta(0)$

In circular motion, the angular speed of the planet is constant. However, in the elliptical motion, the angular speed of the planet is not constant.

Let a time t has passed after $t = 0$. Then, the change in θ_0 of the planet is $\omega_0 t$ whereas the change in θ of the planet won't be the same because of the variation in the angular speed along elliptical trajectory.

Let $\Delta\theta(t) = \theta(t) - \theta_0(t)$.

We know that $\theta_0(t)$ and $\theta(t)$ are periodic by the same time interval, T, as T is the time period of revolution in both the cases (elliptical and circular motion). Hence, all value of $\theta_0(t)$ and $\theta(t)$ repeat after a time period of T. Hence, $\theta_0(t)$ and $\theta(t)$ have a one–to–one relation. Hence, $\Delta\theta$ also repeats after time T. The uniform circular motion thus is a useful approximation because the error $\Delta\theta$ is periodic with time and does not keep accummulating with time to grow to very large values.

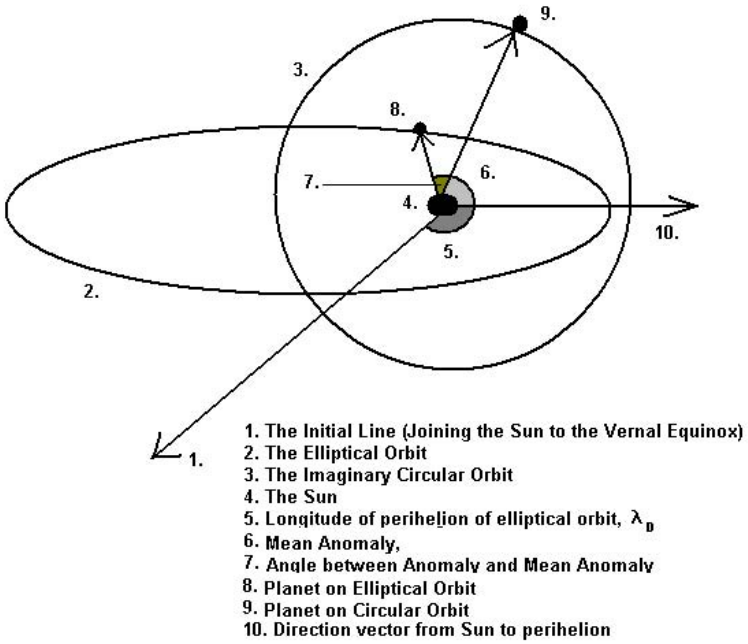

Figure 2. Schematic of the planet in circular and elliptical motion

To find the correction, first consider an elliptical orbit of a planet around the Sun as shown in Fig. 2. We use the equation of the ellipse in polar co-ordinates (r, θ) where θ is the anomaly. The equation of the ellipse then is,

$$r = \frac{l}{1 + e\cos\theta} = \frac{a(1-e^2)}{1 + e\cos\theta} \tag{1}$$

where $l = a(1-e^2)$ is the semi–latus rectum with a as the semi–major axis and e the eccentricity of the ellipse. The semi–minor axis of the ellipse is $b = a\sqrt{(}1-e^2)$.

Now, total area of the ellipse $A = \pi ab$ is swept in T, the time period of revolution. From Kepler's second law we know that the rate of area swept out by the position vector of planet (w.r.t. Sun) is a constant. Therefore the rate of area swept is,

$$\frac{\mathrm{dA}}{\mathrm{dt}} = \frac{r^2}{2}\frac{\mathrm{d}\theta}{\mathrm{dt}} = \frac{\pi ab}{T}$$

Substituting from Equation (1), we get

$$\frac{2\pi}{T} = \frac{(1-e^2)^{\frac{3}{2}}}{(1 + e\cos\theta)^2}\,\frac{\mathrm{d}\theta}{\mathrm{dt}}$$

We notice that $2\pi/T$ is nothing but the mean angular speed ω_0. Therefore

$$\theta_0(t) = \int_0^t \omega_0\,\mathrm{dt} = \int_0^t \frac{(1-e^2)^{\frac{3}{2}}}{(1 + e\cos\theta)^2}\,\mathrm{d}\theta \tag{2}$$

We want to get the equation in the form, $\theta = \theta_0 + \Delta\theta$, so that by adding the longitude of the perihelion on both sides of the equation, we could get the relation between the correct longitude λ and the mean longitude λ_0.

A direct integration of Equation (2) may be very complicated. But we can expand the integrand as a series and integrate only a few first most significant terms. A binomial series expansion is possible because the eccentricity of an ellipse, $e < 1$. Also, during the expansion we drop terms of order e^3 or higher.

$$\theta_0(t) = \int_0^t (1 - \frac{3}{2}\,e^2 + \cdots)(1 - 2\,e\cos\theta + 3\,e^2\cos^2\theta\cdots)\,\mathrm{d}\theta$$

After integraion we get,

$$\theta_0 = \theta - 2\,e\sin\theta + \frac{3}{4}\,e^2\sin 2\theta + \cdots$$

which can be written as

$$\Delta\theta = \theta - \theta_0 = 2\,e\sin\theta - \frac{3}{4}\,e^2\sin 2\theta + \cdots \tag{3}$$

However we want the r.h.s. of Equation (3) to be expressed in terms of θ_0. For that we can substitute $\theta = \theta_0 + \Delta\theta$ on the r.h.s. to get,

$$\Delta\theta = 2\,e\sin(\theta_0 + \Delta\theta) - \frac{3}{4}\,e^2\sin[2(\theta_0 + \Delta\theta)] + \cdots$$

Expanding in powers of $\Delta\theta$ and neglecting terms of order $(\Delta\theta)^2$ or greater (because of their small values) we get,

$$\Delta\theta\,(1 - 2\,e\cos\theta_0 + \frac{3}{2}\,e^2\cos 2\theta_0) = (2\,e\sin\theta_0 - \frac{3}{4}\,e^2\sin 2\theta_0)$$

Again Expanding in powers of e and keeping terms up to e^2, we get,

$$\Delta\theta = 2\,e\sin\theta_0 + \frac{5}{4}\,e^2\sin 2\theta_0 \tag{4}$$

which is the required correction term.

References

[1] Fränz M. and Harper D., Planetary and Space Science, 50, 217 (2002)

[2] Nicholson I., "Unfolding Our Universe", Cambridge University Press (1999)

[3] Simon J. L. et al, Astronomy Astrophysics, 282, 663 (1994)

[4] "The Indian Astronomical Ephemeris for the year 2007", The Indian Meteorological Department, Kolkata (2007)

[5] http://www.hps.cam.ac.uk/starry/mathtechniqueslrg.jpg

P R A Y A S
Students' Journal
of Physics

Bragg-Williams theory of phase transition: Ising model and black hole

Bidyut Prava Nayak
M.Sc., Physics Department, Utkal University, Bhubaneswar, India

Abstract. In this work, we study the phase transitions of two disjoint systems within the Bragg-Williams approximation. First one is the phase transition of system from paramagnetic to ferromagnetic phase. We then use the same approximation scheme to study black hole phase transition in Anti de Sitter space. This is a first order phase transition where there is a crossover from black holes phase to Anti de Sitter phase. We argue that this transition is nicely captured by the Bragg-Williams theory.

Communicated by: L. Satpathy

1. INTRODUCTION

Phase transition is often classified by the behaviour of the order parameter around the transition temperature. While for water-vapour transition the density is the order parameter, for ferromagnetic transitions, it is the magnetisation. As the name suggests, order parameter reflects the order with-in the system. For magnetic system, at high temperature, order is lost among the spins. Hence one gets expectation value of the order parameter to be zero. As we tune down the temperature, at the critical temperature, an order sets in. Consequently, below this temperature, the order parameter is non-zero. Order parameter also helps us to charecterise the nature of the phase transition. Let us denote the expectation value of a generic order parameter by $< \phi >$. While for a system undergoing second order phase transition, $< \phi >$ changes continuously around the critical temperature, for a first order phase transition, the change is rather discontinuous. It also should be mentioned that besides the order parameter, there are few other quantities that are discontinuous around the first order transition point. One of these is the entropy. This is due to the presence of the latent heat during the cross over from one phase to the other.

The purpose of this project is to study two very disjoint systems showing phase transition. One is the Ising model which has enormous impact in understanding phase transition and the other is the phase transition involving black holes. In particular, we will see how Bragg-Williams (will henceforth be called BW) theory apporach helps us bind these two together under a single umbrella. We will, in sequel, also discuss how under certain approximation, BW theory reduces to Landau's mean field theory.

Mean-field theory is an approximation where the order parameter is taken to be spatially constant. In other words, this says that we neglect the spatial fluctuation within the system. Though mean field theory often leads to answers which differ from their actual values, it has always been the first approach taken by reseachers to predict the phase diagrams. There are various formulations of mean field theory, but perhaps the best appreciated one is the Landau's mean field theory approach.

In this project, we start with Ising ferromagnet with in the BW scheme [1]. After discussing the phase diagram, we show how one reproduces Landau's mean field theory approximation from BW energy function. Subsequently, we apply BW approach to describe first order phase transition involving black holes in Anti deSitter space (will be called AdS from now on).

In the rest of this section, we brifly list down certain thermodynamical properties of black holes and also comment about phase transition involving certain black holes [1].

General theory of relativity predicts existence of black holes. They are the sources of extremely large gravitational field. It is often said that the black holes are the objects with-in which things can fall and can not come out. Physicists argued that the end point of collapse of massive starts are black holes. J. Bakenstein and S. Hawking have helped us uncover close relations between thermodynamics and black holes. Below, we list down few general properties of black holes.
(1) Black hole has singularity inside and typically it is shielded by what is known as horizon.
(2) Black holes can be distinguished from each other only by their mass (or equivalently internal energy) M, electric or magnetic charge Q and rotation J. In this project we will consider holes with $Q = J = 0$.
(3) Black hole has surface area (A) which depends on the size of the horizon.
(4) Bakenstein showed us that entropy (S) can be associated with black holes and it is proportional to one-fourth of the horizon area.
(5) Hawking discovered that black hole can also have temperature (T). This temperature is known as Hawking temperature in the literature.
(6) Black hole obeys 0th, 1st and 2nd laws of thermodynamics.

Simplest of these black holes are the Schwarzschild black hole. It is only charectarised by mass/energy. If we take the horizon size r to be given by $r = 2M$ (We here set the Newton's constant $G = 1$. We also will set for simplicity the velocity of lingt c, Boltzman constant k and $\hbar$ also equal to 1.), then

$$A = 4\pi(2M)^2 = 16\pi M^2, \quad S = \frac{A}{4} = 4\pi M^2, \quad T = \frac{1}{8\pi M}. \tag{1}$$

It can be easily checked that the 2nd law of thermodynamics $dU = TdS$ is satisfied since

---

[1] Understanding black hole physics is beyond the scope of this project. However there are certain references which might be useful. See for example [2], [3]. We here list down some well accepted results in black hole physics and do not claim that we understand all these. We will simply use these results as a strating point to build up a model for phase transition.

$$dU = dM \text{ and } TdS = \frac{1}{8\pi M} \times 8\pi M dM. \tag{2}$$

Here are few comments about Schwarzschild black holes. Firstly, we can think of this black holes sitting in Minkowski space. Setting $M = 0$, we have $U = 0$. This is taken to be the energy of the Minkowski's space. Secondly, we note that since themperature is inversely proportional to the mass of the black hole, as energy increases, its temperature decreases. This is typical of theormodynamic systems with negative specific heat. Such systems are generally unstable. Indeed, the Schwarzschild black hole is argued by researchers to be unstable. Because of these reasons we turn our attention to a kind of black holes which are called Schwarzschild black holes in AdS space. We will see that these black holes have positive specific heat with in certain range of parameters.

We will not need to know the details of AdS space but only that it has a constant negative enery density with respect to the Minkowski space. That is why it is often called as negatively curved space time. We will in general assume that this space-time is $1 + n$ dimensional with n space-like and 1 time-like coordinate. Black hole with $M \neq 0, Q = J = 0$ in this space is called AdS-Schwarzschild black holes in literature. We only require the expressions of the energy density, temperature and entropy density of these black holes. They are given by:

$$T = \frac{nr^2 + (n-2)l^2}{4\pi l^2 r}, \tag{3}$$

$$S = \frac{r^{n-1}}{4}, \tag{4}$$

$$E = \frac{(n-1)(r^n l^{-2} + r^{n-2})}{16\pi}. \tag{5}$$

Here r is the horizon radius and l is associated with the energy density of the AdS space. Taking l to infinity would take us to the Minkowski space. Note that for $r \to 0, E \to 0$. $r \to 0$ can be thought of as going to AdS space. This, in turn, means that the energy density has been calculated with respect to the AdS space. The above expressions have appeared in many papers. Here we have taken it from [4]. AdS-Schwarszchild black holes also satisfy various laws of thermodynamics. It can also be seen that for large r, T increases linearly with r (or in otherword with energy). Hence, specific heat in this limit is positive and the black holes are thermodynamically stable. It has been noted earlier by Hawking and Page that AdS-Schwerzschild black hole undergo a first order phase transition from black hole phase to AdS phase as one reduces the temperature below a critical value.

Our aim in this project is to understand this transition with-in the BW approximation. But before we do so, in the next section, we introduce this apporximation via Ising model in n space dimension.

2. ISING MODEL AND BRAGG-WILLIUM THEORY

Ising model is one of the simplest model which is generally used to capture the phase diagram for ferromagnetic to paramagnetic transition. In oder to briefly introduce Ising model, let us consider classical spin variable σ_i sitting at the ith site of a lattice in n dimensional space. σ_i are allowed to

take take vaules $+1$ or -1 representing spin up or spin down states respectively. The coupling is only between two nearest neihgbour spins with strength given by $+J$. With this, we write the Ising Hamiltonian as

$$H = -J \sum_i \sigma_i \sigma_{i+1}. \tag{6}$$

A useful way to chart out the phase diagram that follows from Ising model is the introduce an oder parameter $m =< \sigma >$. At high temperature, one expects $m = 0$ while at low temeprature, an order sets in, leading to $m \neq 0$. We will see in the rest of the section, how a method due to Bragg-Williams helps us to see this behaviour in a very elegant way. We follow [1] in the rest of this discussion. In the next section, we will use this procedure to understand black hole phase transition in AdS space.

Bragg-Williams theory

Let us focus our attention to the magnetic moment of the system just described. One expects the total magnetic moment is proportional to the total number of up spins (N_{up}) and down spins (N_{down}). Assuming the total number of sites as $N = N_{up} + N_{down}$, we expect

$$m = \frac{N_{up} - N_{down}}{N}. \tag{7}$$

Since entropy is defined as the logaritm of number of states, we have

$$S = \ln ({}^N C_{N_{up}}) = \ln ({}^N C_{N(1+m)/2}). \tag{8}$$

After simplification, entropy per unit spin can be re-expressed as

$$s = \frac{S}{N} = \ln 2 - \frac{1}{2}(1+m)\ln (1+m) - \frac{1}{2}(1-m)\ln (1-m). \tag{9}$$

Simplerly the energy per unit spin can be approximated as

$$e = \frac{E}{N} = -\frac{J \sum_i m^2}{N} = \frac{1}{2} J z m^2. \tag{10}$$

Here z is the number of nearest neighbour sites ($z = 2n$ in n dimension). One then construct BW function

$$f(T, m) = e - Ts \tag{11}$$

Using (9) and (10) one gets,

$$f(T, m) = -\frac{1}{2} J z m^2 + \frac{1}{2} T[(1+m) \ln (1+m) + (1-m) \ln (1-m)] - T \ln 2. \tag{12}$$

Behaviour of $f(m, T)$ is shown in figure 1.

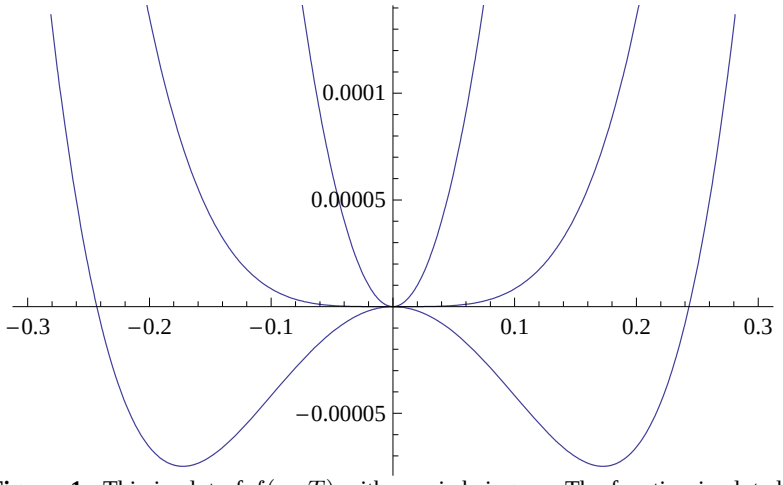

Figure 1. This is plot of $f(m,T)$ with x axis being m. The function is ploted for different values of T/Jz. The top one is for $T/Jz = 1.05$, the middle one is for $T/Jz = 1$ and the lower one is for $T/Jz = .99$.

Note that for $T > Jz$, $f(m,T)$ has a minimum at $m = 0$. For $T < Jz$, minima are for finite non zero values of m. The symmetry in the plot $m \to -m$ is expected due to $\sigma \to -\sigma$ symmetry in Ising Hamiltonian. The shift of the minima from 0 to non-zero values start to occur at $T = T_c = Jz$. T_c is identified as the critical temperature. Since m changes continuously around T_c, we recognise this as a second order phase transition.

To conclude, we have seen in this section that BW theory captures the phase diagram of the Ising model which describes the ferromagnetic transition.

3. LANDAU'S MEAN FIELD THEORY

In the previous section, we constructed the function $f(m,T)$ which describes the phases not only close to $T = T_c$ but also away from it. This is because the magnetisation in $f(m,T)$ can take arbitrary large values. However, as it is obvious that the most interesting region in the phase diagram is around $T = T_c$. In this limit, m is close to zero. Therefore we can expand $f(m,T)$ in powers of m. This leads to

$$f(m,T) = -T \ln 2 + \frac{1}{2}(T - T_c)m^2 + \frac{T}{12}m^4 + \mathcal{O}(m^6). \tag{13}$$

Note that around $T = T_c$, the coefficient of m^2 changes sign. This leads to the change in the location of the minima as we cross T_c. Such a simple power series expansion which captures many interesting physics close to T_c is known as Landau's mean field theory approach towords phase transition. In general, it has a structure

$$f(m,T) = \sum_{i=0}^{\infty} a_i(T)m^i, \tag{14}$$

where a_is are independent of m and generally depende on T. In (13), we have

$$a_0 = T \ln 2, \;\; a_1 = 0, \;\; a_2 = \frac{1}{2}(T - T_c), \;\; a_3 = 0, \;\; a_4 = \frac{T}{12}, \;\; \text{and so on.} \tag{15}$$

In the next section, we will use BW theory to understand the phase transition involving black holes in AdS space.

4. BLACK HOLE PHASE TRANSITION

We are now in a position to apply BW theory for black hole. In (5), we have given the thermodynamic quantities associated with the AdS black hole. Following similar method as in (12), we get

$$f(r,T) = E - TS = \frac{(n-1)(r^n l^{-2} + r^{n-2})}{16\pi} - T\frac{r^{n-1}}{4}. \tag{16}$$

In what follows, we want to treat r as the order parameter. It will play an analogus role of magnetisation m of the last section. To keep things simple, we also set $l = 1$ in the rest of discussion. Though for any $n \geq 4$ our results are going to hold, most recent works in the literarure are for $n = 4$. To understand the behaviour of the function $f(r,T)$, we find out its equilibrium points. This is given by

$$\frac{\partial f}{\partial r} = 0. \tag{17}$$

which gives

$$n - 2 + nr^2 = 4\pi r T, \tag{18}$$

leading to

$$T = \frac{n - 2 + nr^2}{4\pi r}. \tag{19}$$

This is the same expression of temperature (remember here we have set $l = 1$) given in (5). We also see writing (19) is a different way, that for a given temperature, non-zero minimum occurs at

$$r = \frac{2\pi T + \sqrt{2n - n^2 + 4\pi^2 T^2}}{n}. \tag{20}$$

This minimum to exist

$$4\pi^2 T^2 > n^2 - n \tag{21}$$

otherwise the expression in the left hand side of equation (20) will be comples. Finally, substituting the expression of (19) in (16), we get the value of $f(r,T)$ at the extrema. This is nothing but the Helmholz free energy (H). The expression is given by

$$H = \frac{r^{n-2} - r^n}{16\pi}. \tag{22}$$

We note that $H = 0$ for $r = 0$. This will be identified as *no black hole phase* as r is defined as the horizon radius. This is also called simply as the AdS phase. H is also zero for $r = 1$. Between $0 < r < 1,\ H > 0$ and for $r > 1, H < 0$. Since the thermodynamic system will try to minimise H, for $r > 1$, black hole is a stable phase and for $r < 1$, AdS is a stable phase with $r = 0$. This can also be seen if we plot $f(r, T)$ as a function of r for different T. See figure 2. For $T < T_c = 3/(2\pi)$,

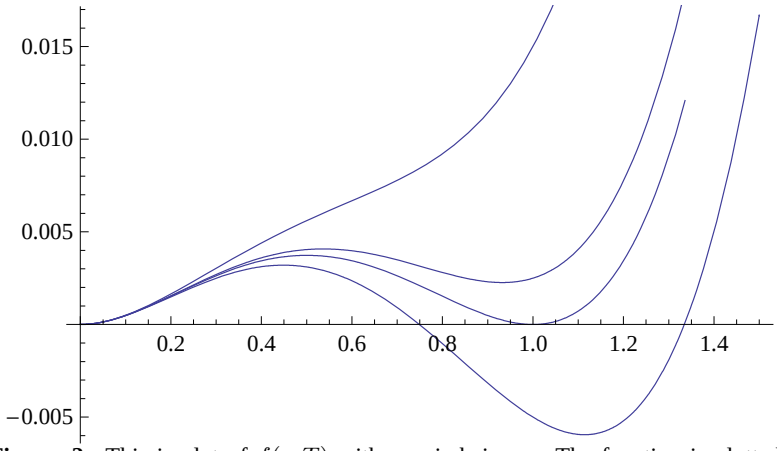

Figure 2. This is plot of $f(r, T)$ with x axis being r. The function is plotted for different values of T. The top one is for $T = .417$, the next one is for $T = .467$. The one with degenerate minima is for $T = T_c = 3/(2\pi) = .47$ and the lowest one is for $T = .497$.

the AdS phase is the stable phase. At $T > T_c$, the black holes phase minimises the BW function. At $T = T_c$ both black hole and AdS phase coexist. The phase diagram is similar to what we expect for water-vapour transition. The density,there, is discontinuous around 100 degree temperature. On the other hand, here, we have discontinious change of r around $T = T_c$. As we increase T beyond T_c, r crosses over from 0 to $r \geq 1$. Consequently, entropy also jumps around T_c (we note that black hole entropy is proportional to r). From these properties, we conclude that this is a *first* order phase transition. It was discovered by Hawking and Page in 1983 in their studies of black hole in AdS space.

5. CONCLUSION

To conclude, we have seen that BW theory helps to understand phase transitions appearing in two completely different areas in physics. These are:

(1) Ising model of ferromagnetic to paramagnetic transition. This is a second order phase transition.
(2) Transition in gravity theories from ordinary phase (or Anti deSitter phase) to a black hole phase. This is an example of first order phase transition.

While in one case, magnetisation works as the order paraneter, for black hole, it is the horizon radius acts as the order parameter.

ACKNOWLEDGEMENTS

I express my heartiest gratitude and appreciation to my guide Sudipta Mukherji whose proper guidance and encourangement helped me a lot to finish my project. I really enjoyed working for this project. This is due to the friendly behaviour and the best co-operation of my guide. It is a memorable thing in my life to work with him. I am grateful to the Institute of Physics for selecting me as a summer project student.I am also thankful to all the members of IOP for their co-operation. I thank my parents for their moral support and co-operation.

References

[1] P.M. Chaikin and T.C. Lubensky, *Principles of condensed matter physics*, Cambridge University Press, 1995, Chapter 4.

[2] B.R. Parker and R. J. McLeod, *Black hole thermodynamics in an undergraduate course*, Am.J.Phys 48, 1066,1980.

[3] J. Orear and E.E. Salpeter, *Black Holes and Pulsers in the introductory physics course*, Am.J.Phys 41, 1131, 1973.

[4] E. Witten, *Anti-de Sitter space, thermal phase transition, and confinement In gauge theories*, Adv.Theor.Math.Phys.2:505-532,1998.

P R A Y A S
Students' Journal
of Physics

Order Parameter Space With Point Group Symmetry

Shreyas Patankar
Chennai Mathematical Institute, Padur P.O., Chennai - 603 103*

Abstract. The stability of topological structures (defects, textures, etc.) in an ordered medium depends on the non-triviality of homotopy groups of the order parameter space for that medium. If the order parameter is taken to be the orientation of a molecule, then the homotopy groups are closely related to the isometry subgroups for that molecule. We consider the case for which the isometry subgroup is discrete, in particular, the cases where the molecule has triangular prismatic, and tetrahedral symmetry. In both cases, the fundamental group for the media is found to be non-Abelian, further, the elements of the groups can be split into six distinct conjugacy classes for the prism and seven for the tetrahedron, giving rise to six and seven possible distinct non-trivial topological structures respectively.

Communicated by .....

1 INTRODUCTION

In an ordered medium, the stability of topological structures (defects, textures etc.) is determined by the successive homotopy groups of the order-parameter space R for the medium [1]. Consider a medium such as a liquid crystal, where the order parameter is the orientation of the individual liquid crystal molecule.

2 FUNDAMENTAL GROUP

The orientations of the molecule can be given by the full group of rotations in 3 dimensions: $SO(3)$. However, suppose that the molecule has an isometry subgroup H, that is, it remains invaraint under any of the transformations in H. (Recall that in an ordinary (nematic) liquid crystal, the isometry subgroup is $SO(2)$, the group of rotations about the z axis, together with π rotaions about x axis.) Then, the order parameter space can be represented as the quotient group $R = SO(3)/H$[1]. Henceforth, we shall assume that H is a finite subgroup.

*shreyas@cmi.ac.in

It is convenient for further calculations if the order parameter space is written as $R = G/H$, where G is simply connected.

Consider the group of unit quaternions represented as $SU(2)$. Suppose we write $u \in SU(2)$ as $u(\hat{n}, \theta) = \cos\left(\frac{\theta}{2}\right) + \hat{n} \cdot \vec{\sigma} \sin\left(\frac{\theta}{2}\right)$, where $\hat{n}$ is a unit vector in three dimensions and σ_i are the basis quaternions. The $SU(2) \rightarrow SO(3)$ homomorphism can be written as $\phi(u(\hat{n}, \theta)) = T(\hat{n}, \theta)$, T denoting the 3 dimensional rotation about the axis $\hat{n}$ by an angle θ[1].

Thus, if $\tilde{H} = \phi^{-1}(H)$, then we can write $R = SU(2)/\tilde{H}$, with the added advantage that $SU(2)$ is simply connected.

By the theorem on short exact sequences[1], the fundamental group of R is given by $\pi_1(SU(2)/\tilde{H}) = \pi_0(\tilde{H}/\tilde{H}_0)$ ...($\tilde{H}_0$ being the connected component of the identity of $\tilde{H}$).
As $\tilde{H}$ is finite, $\tilde{H}_0$ is trivial, and hence, $\pi_0(\tilde{H}/\tilde{H}_0) = \tilde{H}$. Thus, $\pi_1(SU(2)/\tilde{H}) = \tilde{H}$

We know that $SU(2)$, being a Lie group, is also 2-simple and hence, $\pi_2(R) = \pi_1(\tilde{H}) = 0$ as $\tilde{H}$ is discrete. Thus, we see that the order parameter space is also 2-simple and cannot have stable point defects (in 3 dimensions) or textures (in 2 dimensions).

3 CONJUGACY CLASSES[1]

By definition, the fundamental group of a space R is defined to be the collection of homotopy classes of loops that are *based at a point* $x \in R$. However, note that if γ_1 and γ_2 are two loops in R characterizing the same defect, then γ_1, γ_2 need only be *freely homotopic*, that is, they should be continuously deformable to each other without being constrained to any fixed base point. It can be shown[1] that if f and g are two loops based at a point $x \in R$ that belong to distinct homotopy classes, and if $c \in \pi_1(R, x)$ is any other loop based at x such that $g = cfc^{-1}$, then f and g are freely homotopic to each other.

In the group $\pi_1(R)$, the set of all elements g such that $g = cfc^{-1}$ for $c \in \pi_1(R)$ is called the *conjugacy class* of f,sometimes written as $\{f\}$. Thus, distinct topological objects are characterised by distinct *conjugacy classes* of $\pi_1(R)$.

4 STANDARD EXAMPLES: LIQUID CRYSTALS[2]

41 Nematic liquid crystals

Let us now consider two standard examples of determining topological structures using the fundamental group: that of liquid crystals. A nematic liquid crystal molecule has full rotation symmetry,

---

[1]This section is a summary of arguments provided by Mermin, (1979)
[2]Summary of results presented by Mermin, (1979)

along with π rotation symmetry along a perpendicular axis. (The symmetry group is same as that for a cylinder). Thus, the symmetry group is $SO(2)$ together with antipodal points identified, that is $H = D_\infty$. The lift $\tilde{D}_\infty$ has two connected components. Thus, $\pi_1(SU(2)/\tilde{D}_\infty) = \pi_0(\tilde{D}_\infty) = Z_2$. Thus, a nematic liquid crystal can have two non-trivial topological defects. Further, as the fundamental group is abelian, the defects are not equivalent.

42 Biaxial Nematics

Another standard example is that of biaxial nematic liquid crystal, whose molecules have the symmetry group of a rectangular box. The order parameter space can thus be written as $R = SO(3)/D_2$, where D_2 is the dihedral symmetry group of a rectangular box. The lift of D_2 from $SO(3)$ to $SU(2)$ turns out to be isomorphic to the quaternion group $Q = \{\pm 1, \pm\sigma_1, \pm\sigma_2, \pm\sigma_3\}$ The fundamental group of $R = SU(2)/Q$ is then simply $\pi_1(R) = Q$ which is non-Abelian. It can be easily seen that the 8 elements of this group split into five distinct conjugacy classes: $\{+1\}, \{-1\}, \{\pm\sigma_1\}, \{\pm\sigma_2\}, \{\pm\sigma_3\}$ Thus a biaxial nematic can have five distinct, stable topological structures.

43 Triangular prismatic symmetry

Let us consider an order parameter which has the triangular prismatic (also known as 'dihedral') symmetry group. This can be, for instance, the orientation of a molecule that has triangular prismatic symmetry. We can write the order parameter space as $R = SO(3)/D_t$, where D_t is the dihedral symmetry group for a triangular prism.

We wish to characterise the dihedral symmetry group. Obviuosly, this group has six elements. Consider a coördinate system with the origin at the center of a triangular prism, the z axis along the axis of the triangles, and the x-axis perpendicular to one of the 'long' edges. Suppose we denote a $\frac{2\pi}{3}$ rotation about $\hat{z}$ by q, and a π rotation about $\hat{x}$ by p. Then, we claim that $1, p, q$ are generators for the group D_t. Evidently, q, p satisfy $p^2 = 1$ and $q^3 = 1$. Further, it is also easy to show that they are interrelated by the relation $qp = pq^2$

Thus, every element $r \in D_t$ can be expressed as $r = j^x\omega^y$, where $x \in \{0, 1\}$ and $y \in \{0, 1, 2\}$, implying that p, q are generators of D_t

Suppose $\tilde{D}_t$ be the inverse image of D_t under the $SU(2) \to SO(3)$ homomorphism ϕ, and let the preimages of the generators $1, p, q$ be $\pm 1, \pm j \pm \omega$ repectively. Then, from construction, we have that,

$j = \sigma_1$

$\omega = -\frac{1}{2} + \frac{\sqrt{3}}{2}\sigma_3$

Observe that j, ω satisfy the relations

$j^2 = -1, \omega^3 = +1$ and $\omega j = +j\omega^2$

Thus, any $x \in \tilde{D}_t$ can be written as $x = \pm j^x \omega^y$ where $x \in \{0, 1\}$ and $y \in \{0, 1, 2\}$, implying that j, ω are generators of $\tilde{D}_t$

We can now easily classify the (12) elements of $\tilde{D}_t$ into conjugacy classes as:

$\{1\}$

$\{-1\}$

$\{\omega, \omega^2\}$

$\{-\omega, -\omega^2\}$

$\{j, j\omega, j\omega^2\}$

$\{-j, -j\omega, -j\omega^2\}$

Thus we have five distinct, nontrivial conjugacy classes whcih in turn correspond to five distinct classes of nontrivial topological structures.

As an illustration consider a loop l in physical space that corresponds to the element j of the fundamental group. Further, suppose x is a defect in physical space corresponding to the element ω of the fundamental group. Now consider the resultant topological structure formed by moving the defect x along the path l. Then this is equivalent to the loop $y = j\omega j^{-1} = j\omega(-j) = \omega^2$. Thus, moving a ω-defect around a j-defect results in a defect that is equivalent to ω^2. Hence, as expected, the defects ω, ω^2 are not distinct and belong to the same conjugacy class.

44 Tetrahedral symmetry

Now consider an order parameter which has the tetrahedral symmetry group. Then we can write the order parameter space as $R = SO(3)/T$, where T is the tetrahedral symmetry group.

Thus, the isometry subgroup is the tetrahedron symmetry group T, which is known to be isomorphic to the alternating group A_4[2], that is, the group of even permutations of four distinct letters. It has been found that T written as a subgroup of the permutatino group S_4 can be generated by three

permutationo elements together with the identity [2] which we shall call p, q, r. In the cycle notation [3], these generators can be written as $1, p = (ab)(cd), q = (ac)(bd), r = (abc)$ and they satisfy the relations,

$p^2 = q^2 = 1$, $r^3 = 1$, $qp = pq$, $rp = pqr$ and $rq = pr$

If we represent the isometric rotations of a tetrahedron by permutations of the vertex labels, the rotations may be represented as shown (fig. 1)

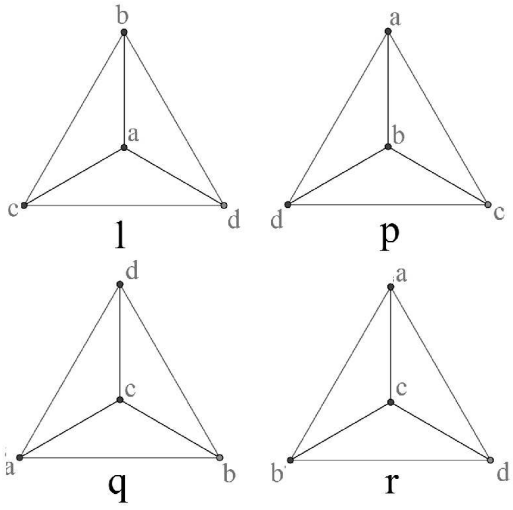

Figure 1. Tetrahedron group generators

We shall describe these rotations geometrically as $p = R(\hat{m}, \pi)$, $q = R(\hat{n}, \pi)$, $r = R\left(\hat{i}, \frac{2\pi}{3}\right)$ (with the origin at the centre of the tetrahedron and the x-axis aligned towards the vertex d. $\hat{m}$ is the axis joining the midpoint of cd to that of ab, and $\hat{n}$ is the asis joining midpoint of ac to that of bd). The axes $\hat{m}$ and $\hat{n}$ are given as:

$$\hat{m} = -\frac{1}{\sqrt{3}}\hat{i} - \frac{1}{\sqrt{6}}\hat{j} + \frac{1}{\sqrt{2}}\hat{k}$$
$$\hat{n} = \frac{1}{\sqrt{3}}\hat{i} + \frac{1}{\sqrt{6}}\hat{j} + \frac{1}{\sqrt{2}}\hat{k}$$

Thus, any element $m \in A_4$ can be written as $m = p^x q^y r^z$, where $x, y \in \{0, 1\}$ and $z \in \{0, 1, 2\}$. (As expected, the total number of elements in the group is $2 \cdot 2 \cdot 3 = 12$)

It has also been shown [2] that the elements of this group fall into four conjugacy classes:

$\{1\}$

$\{p, q, pq\}$

$\{r, pr, qr, pqr\}$

$\{r^2, pr^2, qr^2, pqr^2\}$

45 Lift of A_4 in $SU(2)$

As shown above, we are primarily concerned with the lift $\tilde{T}$ of A_4 in $SU(2)$. We know that the homomorphism ϕ maps $\pm u \in SU(2)$ to a single element $R \in SO(3)$. Thus, let us denote the preimages of $1, p, q, r$ as $\pm 1, \pm\alpha, \pm\beta, \pm\gamma$. As $1, p, q, r$ are generators for the group T, their preimages are generators of the group $\tilde{T}$

Thus, we have

$$\alpha = -\frac{1}{\sqrt{3}}\sigma_1 - \frac{1}{\sqrt{6}}\sigma_2 + \frac{1}{\sqrt{2}}\sigma_3$$
$$\beta = \frac{1}{\sqrt{3}}\sigma_1 + \frac{1}{\sqrt{6}}\sigma_2 + \frac{1}{\sqrt{2}}\sigma_3$$
$$\gamma = -\frac{1}{2} + \frac{\sqrt{3}}{2}\sigma_1$$

and we can trivially verify the generator relations,

1. $\alpha^2 = \beta^2 = -1$ and $\gamma^3 = +1$
2. $\beta\alpha = -\alpha\beta$
3. $\gamma\alpha = \alpha\beta\gamma$
4. $\gamma\beta = -\alpha\gamma$

Thus, now for any $x \in \tilde{T}$, we can write $x = \alpha^x\beta^y\gamma^z$, with $x, y \in \{0, 1\}$ and $z \in \{0, 1, 2\}$. Obviously, this verifies that $o(\tilde{T}) = 24$

46 Conjugacy classes

The group $\tilde{T}$ written in terms of its generators can be split into the conjugacy classes:

$\{1\}$

$\{-1\}$

$\{\alpha, -\alpha, \beta, -\beta, \alpha\beta, -\alpha\beta\}$

$\{\gamma, -\alpha\gamma, \beta\gamma, -\alpha\beta\gamma\}$

$\{-\gamma, \alpha\gamma, -\beta\gamma, \alpha\beta\gamma\}$

$\{\gamma^2, \alpha\gamma^2, -\beta\gamma^2, \alpha\beta\gamma^2\}$

$\{-\gamma^2, -\alpha\gamma^2, \beta\gamma^2, -\alpha\beta\gamma^2\}$

To illustrate, consider a loop l in physical space that corresponds to the element α of the fundamental group. Further, suppose x is a defect in physical space corresponding to the element γ of the fundamental group. Now consider the resultant topological structure formed by moving the defect x along the path l. Then this is equivalent to the loop $y = \alpha\gamma\alpha^{-1} = \alpha\gamma(-\alpha) = +\beta\gamma$ Thus, moving a γ-defect around a α-defect results in a defect that is equivalent to $\beta\gamma$ Hence, as expected, the defects $\gamma, \beta\gamma$ are not distinct and belong to the same conjugacy class.

Thus we have six distinct, nontrivial conjugacy classes whcih in turn correspond to six distinct classes of nontrivial topological structure.

5 CONCLUSION

It has been shown (Mermin, 1979) that in a medium, arbitrary entangled line defects can be seperated if and only if the fundamental group of the order parameter space is Abelian. If two distinct line defects entangle in a medium with Abelian fundamental group, they can cross each other spontaneously, removing the entanglement. Thus, over time, line defects (in, for example, a nematic liquid crystal) tend to smoothen out over time. However, in a medium with non-Abelian fundamental group, seperating entanglements will give rise to further defects, and hence over time, the medium will have more defects and more entanglements.

In the standard example of a biaxial nematic, two entagled line defects from distinct conjugacy classes can not be seperated without leaving any trace. In the two examples that have been considered, the richer structure of the conjugacy classes implies that it is even less likely for two arbitrary entangled defects to be seperated without any trace. It has been stated (Mermin, 1979) that the property of entangled defects passing through each other can affect the elasticity of the medium.

Acknowledgements

If needed, then write the acknowledgements here.

References

[1] Mermin, N. D., 1979, *The topological theory of defects in ordered media*, Reviews of Modern Physics, Vol. 51

[2] Beach, J. A., W. D. Blair, 1996, *Abstract Algebra* (2nd ed.), Waveland Press

[3] Weisstein, Eric W. “Permutation Cycle” From *MathWorld*–A Wolfram Web Resource

PROBLEMS IN PHYSICS

Readers are invited to submit the solutions of the problems in this section within two months. Correct solutions, along with the names of the senders, will be published in the alternate issues. Solutions should be sent to: H.S. Mani, c/o A.M. Srivastava, Institute of Physics, Bhubaneswar, 751005; e-mail: ajit@iopb.res.in

Problems set by H.S. Mani

1. Consider an infinite parallel plate capacitor made of two plates carrying a surface charge density σ_1 and σ_2 ($\sigma_1 = \sigma_{i1} + \sigma_{o1}$ where σ_{i1}, σ_{o1} are the charges per unit area of the inner and the outer surfaces of the firsst plate with a similar expression $\sigma_2 = \sigma_{i2} + \sigma_{o2}$ for the other plate. Find the charge distribution ($\sigma_{i1}\sigma_{o1}\sigma_{i2}\sigma_{o2}$ on the four surfaces in terms of σ_1 and σ_2. (we are taught the special case when $\sigma_1 + \sigma_2 = 0$, in which case the charge resides only on the inner surface of the parallel capacitor.)

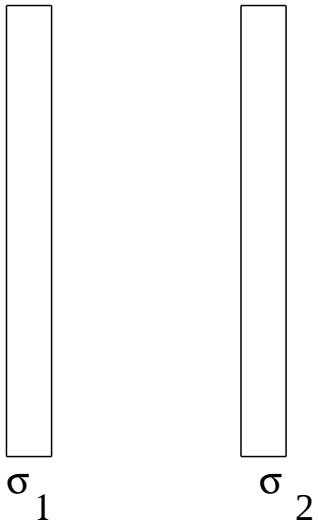

Prob 1.

2. Consider two magnetic dipoles $\vec{\mu}_1$ and $\vec{\mu}_2$, the first one pointing along the $y-$ direction (that is $\vec{\mu}_1 = \mu_1\hat{j}$)and kept at the origin $\vec{r}_1 = 0$and the second pointing along the x-direction (that is $\vec{\mu}_2 = \mu_2\hat{i}$) and is located at $\vec{r}_2 = d\hat{j}$We knowthat the torque acting on a magnetic moment $\vec{\mu}$ is given$\vec{\mu} \times \vec{B}$ where $\vec{B}$ is the extermal magnetic field.Now notice that the magnetic field due to $\vec{\mu}_1$ at $\vec{r}_2$ is along $-\hat{j}$ and hence the torque on $\vec{\mu}_2$is along $-\hat{k}$. The magnetic field due to $\vec{\mu}_2$ at the origin is along $\cap i$ and hence the torque on $\vec{\mu}_1$ is also along $-\hat{k}$. This means both the dipoles rotate so that their total angular momentum is along $-\hat{k}$. However initially they are at rest and carry no initial angular momentum. How do you reconcile this with conservation of angular momentum?

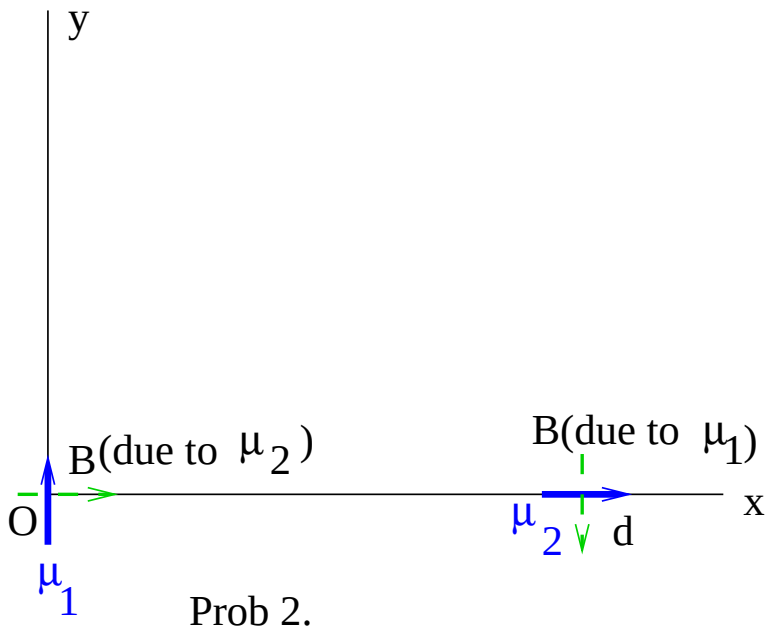

Prob 2.

Solutions to the problems given in Vol.3 No.4

Solutions provided by H.S. Mani

Problem 1:

(a) An electric dipole of strength P produces radiation when it oscillates with an angular frequency ω. Here we are considering the dipole as an one dimensional oscillator. Using the fact that the energy density in an electric field E is proportional to $\epsilon_0 E^2$, find the power radiated by the oscillator using dimensional analysis. (upto a numerical factor)

(b) Consider the Hydrogen atom in which the electron goes around the proton in a circular orbit of radius $5 \times 10^{-11} m$. If the emitted radiation is due to the classical formula find the time it will take to reach the proton. (assume the radius of the proton to be $10^{-15} m$). Assume the orbit circular as it spirals down.

(c) Consider a binary star system radiating gravitational energy because of its motion around each other in a circular of radius R about their centre of mass. First, prove the dipole moment for mass vanishes about the centre of mass. Then use the relevent physical variable to write an expression for the power emitted by the system.

(d) How would the answer be modified for the case of a charged particle moving in an elliptical orbit (semi-major axis is a and the semi-minor axis is b) for the case of electromagnetic radiation? (one could also obtain the formula for the gravitaional radiation by treating the elliptical motion as circular in infinitesimal parts and perform an integration over the ellipse) The formula derived using the general theory of relativity was tested for the binary pulsar PSR 1913+16 by R.A.Hulse and J.H.Taylor. They were awarded the Nobel Prize in 1993 .

Solution to Problem 1:

(a) The electric field is proportional to $P/(4\pi\epsilon_0)$ and so the energy density is proportional to $P^2/(4\pi\epsilon_0)$ (where we have dropped a factor of 4π) and so this whould be a factor in the result. The other variables are ω and the velocity of light c as the wave travels with the speed of light (note power radiated per unit area is energy density$\times$ velocity.) Thus we write

$$Power \;\; radiated = (P^2/(4\pi\epsilon_0))c^\alpha \omega^\beta \tag{1}$$

where α and β are to be deterimned by dimesional analysis. This is easily done as (Length=L;Time=T)

$$Power \;\; radiated = Energy/T \tag{2}$$

and if q is the charge then using $P = qL$,

$$\frac{P^2}{4\pi\epsilon_0} = \frac{q^2}{4\pi\epsilon_0 L} L^3 = Energy \times L^3 \tag{3}$$

Using the dimensions of $c = L/T$ and $\omega = T^{-1}$, we get $\alpha = -3$ and $\beta = 4$ giving

$$Power \;\; radiated = N\frac{P^2\omega^4}{4\pi\epsilon_0 c^3} \tag{4}$$

Where N is a numerical constant. The complete treatment based on electrodynamics gives $N = \frac{1}{3}$.

(b) In hydrogen atom, the electrons circular motion can be thought of as two harmonic oscillators moving perpendicular to each other and each radiating an amount given by Eq.(4) and so the energy lost $-\frac{dE}{dt}$ due to radiation is, where E is the energy of the hydrogen atom is

$$\frac{2}{3}\frac{P^2\omega^4}{4\pi\epsilon_0 c^3} \tag{5}$$

For a hydrogen atom moving in a circular orbit of radius r the energy E is the sum of potential energy $-e^2/(4\pi\epsilon_0 r)$ and kinetic energy $mv^2/2$ where e, m and v are the charge and the mass of the electron and its speed respectively. We also have $mv^2/r = e^2/(4\pi\epsilon_0 r^2)$. Using these we get

$$E = -\frac{e^2}{8\pi\epsilon_0 r} \tag{6}$$

This leads to

$$\frac{dE}{dt} = \frac{e^2}{8\pi\epsilon_0 r^2}\frac{dr}{dt} = -\frac{2}{3}\frac{e^2 r^2\omega^4}{4\pi\epsilon_0 c^3} \tag{7}$$

where we have used $P = er$ in tha above equation. Using

$$\omega = (\frac{e^2}{4\pi\epsilon_0 m r^3})^{1/2} \tag{8}$$

and Eq.(7) we get

$$\frac{dr}{dt} = \frac{4}{3}\frac{(\frac{e^2}{4\pi\epsilon_0 m})^2}{r^2 c^3} \tag{9}$$

this can be integrated to obtain the time T taken for the electron to move from $r = 5\times 10^{-11}m$ to $10^{-15}m$ as

$$T = \frac{((5\times 10^{-11})^3 - (10^{-15})^3)c^3(4\pi\epsilon_0 m)^2}{4e^4} \tag{10}$$

this works out to $T = 3.4\times 10^{-13}s$.

This was one of the arguments used against classical physics as hydrogen atom is stable.

(c) For a binary system of masses m_1 and m_2 located at $\vec{r}_1$ and $\vec{r}_2$ respecitively the centre of mass $\vec{r}_{c.m}$is at $(m_1\vec{r}_1 + m_2\vec{r}_2)/(m_1 + m_2)$. the dipole moment about any point $\vec{R}$ is defined as

$$(m_1(\vec{r}_1 - \vec{R}) + m_2(\vec{r}_2 - \vec{R})/(m_1 + m_2) \tag{11}$$

This equals

$$\vec{r}_{c.m} - \vec{R} \tag{12}$$

which vanshes when $\vec{R} = \vec{r}_{c.m}$.

However the quadrupole moment does not vanish. Again from the analogy of electromagnetisc radiation we expect the gravitational radiation to be proportional to Q^2, where Q denotes the strngth of the quadrupole. The dimension of quadrupole is $M \times L^2$, M being the dimensions of mass. We write the formula for the power emitted ,

$$Power \;\; emitted = N_g Q^2 G^\alpha \omega^\beta c^\gamma \tag{13}$$

where G is the Newton's gravitational constant and N_g a numerical constant, which can not be determined by dimensional considerations. It is easy to verify $\alpha = 1, \beta = 6$ and $\gamma = -5$, giving us

$$Power \;\; radiated = N_g \mu^2 R^4 G \omega^6 / c^5 \tag{14}$$

where we have replaced Q by μR^2 as the quadrupole moment (μ is the reduced mass). The constant N_g can only be obtained from General Theory of Relativity.

Note in this case we can multiply this by the dimensionless quantity $\Pi = QG\omega^3/c^5$ or any funtion of Π. The expression Eq.(14) also uses the fact that the power radiated is proportional to Q^2. Something besides dimensional analysis is needed to get the result. The numerical constant is $N_g = 6.4$.

(d) In the case of an ellptic orbit we have two harmonic oscillators of strength ea and eb. and thus the power would be

$$\frac{1}{3}\frac{e^2(a^2+b^2)\omega^4}{4\pi\epsilon_0 c^3} \tag{15}$$

If we use eccentricity parameter e defined by $b^2 = a^2(1-e^2)$,we get the expression for the power radiated as

$$\frac{2(1-e^2/2)}{3}\frac{e^2a^2\omega^4}{4\pi\epsilon_0 c^3} \tag{16}$$

For the case of gravitational radiation see a recent article by C.Bracco,J.P.Provost and P.Salati in ArXives (0811.0317)

Problem 2:

There is a famous analysis of G.I.Taylor, a British scientist who obtained the energy liberated by an atom bomb detonated (referred to as Trinity) by studying pictures from Life magazine, which had published the mushroom developing at different times. This was obtained by using dimensional analysis and an ingenious choice of variables. (This was done in late 1940's when the enrgy released was still a classified information). This has been converted into a problem (with hints)

Consider an explosion releasing a large amount of energy. Assume the shock wave produced in the atmosphere is hemispherical. Find the radius R as a funtion of the time t after explosion in terms of the energy E released and other physical quantities relevent to the atmosphere and use dimensional analysis. (Use the fact theat energy released is large and the time in which the shockwave expands is very small)

Solution to Problem 2:

The relevent physical quantities are the energy released E, time after the explosion t, the density of air ρ_0, the atmospheric pressure P_0 and r the radius of the shockwave. One can form two dimensionless constants using the above quantities Π_1 and Π_2 defined by

$$\Pi_1 = r(\frac{\rho_0}{t^2 E})^{\frac{1}{5}}; \Pi_2 = P_0(\frac{t^6}{E^2\rho_0^3})^{\frac{1}{5}} \tag{17}$$

therefore r can be written as

$$r = (\frac{t^2 E}{\rho_0})^{\frac{1}{5}} F(\Pi_2) \tag{18}$$

where F is any function of Π_2. Uptill now only straight forward dimensional analysis has been used. Now Taylor assumed that in the atomic explosion E, the energy released is very large and and time t is very short and so Π_2 is a very small number and he appoximated Eq.(18) by

$$r = (\frac{t^2 E}{\rho_0})^{\frac{1}{5}} F(0) = N_a(\frac{t^2 E}{\rho_0})^{\frac{1}{5}} \tag{19}$$

Where N_a is numerical constant. Since r as a function of t was known from the pictures published in the Life magazine and the value of $\rho_0 = 1.25 kg/m^3$, the only unknown quantity was the energy released E in Eq.(19). Taylor got the result as 21 kilotons of TNT. (1 kilo of TNT= $4.18 \times 10^{12} Joules$) This value was within 10% of the actual value. When Taylor had obtained the value using the simple analysis described above, the actual value was classified.